

# POISSON QUADRATURE METHOD OF MOMENTS FOR 2D KINETIC EQUATIONS WITH VELOCITY OF CONSTANT MAGNITUDE

YIHONG CHEN, QIAN HUANG\*, WEN-AN YONG, AND RUIXI ZHANG

**ABSTRACT.** This work is concerned with kinetic equations with velocity of constant magnitude. We propose a quadrature method of moments based on the Poisson kernel, called Poisson-EQMOM. The derived moment closure systems are well defined for all physically relevant moments and the resultant approximations of the distribution function converge as the number of moments goes to infinity. The convergence makes our method stand out from most existing moment methods. Moreover, we devise a delicate moment inversion algorithm. As an application, the Vicsek model is studied for overdamped active particles. Then the Poisson-EQMOM is validated with a series of numerical tests including spatially homogeneous, one-dimensional and two-dimensional problems.

## 1. INTRODUCTION

In this work we are interested in kinetic equations with velocity of constant magnitude (KE-VC). Such equations can be used to describe the motion of overdamped active particles with self-propulsive forces of a constant magnitude [2, 9, 17, 18]. Among KE-VC are also the radiative transfer equations of photons and neutrons [7, 21]. Besides, such kinetic equations arise in the ‘semi-continuous’ discretization of the Boltzmann equation with the velocity space replaced by a series of spheres [25].

Like the usual kinetic equations, the KE-VC is computationally costly due to the high dimensionality. Thus, the method of moments as a model reduction technique attracts much attention. This method provides a successful bridge connecting the kinetic equation to the hydrodynamic theory [11, 19] (see also [2, 9, 17] for a well-known active particle system). The resultant systems have clear physical interpretations for the lower-order moments, are computationally more feasible, can be valid over a wider range of flow regimes, and naturally inherit the conservation laws of the kinetic equation. The existing moment methods for KE-VC include the classical  $P_N$  method (using the spherical harmonics as the basis) [24] and the maximum entropy (or termed  $M_N$ ) method [22]. However, these methods still cause computational difficulties or generate unphysical results in some cases [3]. Therefore, developing effective moment methods remains an active research direction.

This work is an attempt in this direction. It is inspired by the extended quadrature method of moments (EQMOM) originally proposed for the Boltzmann equation [4]. In EQMOM, the distribution is approximated as a sum of several homoscedastic kernels with independent weights and centers. It thus preserves positivity of the distribution, and the parameters (weights, centers and variance) can be efficiently computed [23, 19]. For the one-dimensional velocity, the Gaussian distribution is most-widely used as the kernel [5]. The EQMOM has also become a popular method to simulate the evolution of aerosol size and compositional distributions using the lognormal or Gamma distribution (supported on  $\mathbb{R}_+$ ) and the compactly-supported beta distribution as kernels, respectively [23, 16, 31]. Further discussions and multidimensional extensions of EQMOM can be found in [5, 15, 14, 32].

We aim in this work to develop a new method of moments for the 2D KE-VC by using the Poisson kernel. This seems the first time to pick the Poisson kernel as a building block in the moment method.

---

2020 *Mathematics Subject Classification.* Primary 35F50 · 35Q82 · 82-10.

*Key words and phrases.* kinetic equation, moment method, Poisson kernel, active matter, Vicsek model.

\* Corresponding author.

This work is supported by National Key Research and Development Program of China (Grant no. 2021YFA0719201) and National Natural Science Foundation of China (Grant no. 12071246).

Previously, the Poisson kernel was adopted as ‘components’ in the statistical mixture model but irrelevant to the kinetic equation [30]. The Poisson kernel was also involved in a discretized spectral approximation method in the one-dimensional neutron transport theory [27], which is different from our attempt. On the other hand, to our best knowledge, the reported combinations of EQMOM with KE-VC are only for the one-dimensional radiative transfer equations [1, 29]. As such, our method, denoted Poisson-EQMOM, is a novel way to formulate hydrodynamic theories of planar flows for overdamped active matter.

The Poisson-EQMOM naturally inherits from EQMOM the advantages of *being positivity-preserving* (which cannot be satisfied by the  $P_N$  method) and *having a conservative form*. Surprisingly, we show in Theorem 2.1 that the derived moment closure systems are well defined for *all physically relevant moments*, while the existing EQMOM variants may not have such a global property [5]. More importantly, the resultant approximations of the distribution function *converge* as the number of moments goes to infinity (see Theorem 2.2). This convergence is desired for any moment method but has not been demonstrated for other quadrature-based method of moments. These properties indicate that the Poisson kernel is a very right choice for the EQMOM to handle KE-VC. On the basis of these nice properties, we devise an efficient and robust moment inversion algorithm while the existing ones [23, 19] seem not work in certain situations.

As an application, we apply the Poisson-EQMOM to a 2D KE-VC derived from the Vicsek dynamics [9] and obtain a moment closure system. The system is solved numerically with a detailed calculation of the kinetic-based flux. The results for five different cases, ranging from spatially homogeneous to 2D, are all quite satisfactory in comparison with analytical results, macroscopic solutions and microscopic particle simulations [13].

The remainder of the paper is organized as follows. Section 2 presents the Poisson-EQMOM with its realizability and convergence properties, one of which is proved in Appendix A. The moment inversion algorithm is developed in Section 3. Section 4 is devoted to the application of the Poisson-EQMOM to a KE-VC from the Vicsek model. A numerical scheme is given in Section 5, whereas the numerical results are reported in Section 6. Conclusions are drawn in Section 7.

## 2. MOMENT METHOD WITH POISSON KERNEL

Consider the 2D KE-VC for an angular distribution  $f = f(t, \mathbf{x}, \theta)$  with  $t > 0$ ,  $\mathbf{x} \in \mathbb{R}^2$  and  $\theta \in \mathbb{R}$  (modulo  $2\pi$ ):

$$\partial_t f + v_0 \mathbf{e}_\theta \cdot \nabla_{\mathbf{x}} f = Q(f). \quad (2.1)$$

Here  $v_0$  is a constant speed,  $\mathbf{e}_\theta = (\cos \theta, \sin \theta) \in S^1$ , and  $Q(f)$  is a problem-specific collision operator. A typical example for the polar active flow will be detailed in Section 4.

Our goal is to develop a moment method for solving the above kinetic equations. For this purpose, we define the  $k$ th angular moments of  $f(t, \mathbf{x}, \theta)$  as

$$c_k = c_k(t, \mathbf{x}) = \int_{-\pi}^{\pi} f(t, \mathbf{x}, \theta) \cos k\theta d\theta, \quad s_k = s_k(t, \mathbf{x}) = \int_{-\pi}^{\pi} f(t, \mathbf{x}, \theta) \sin k\theta d\theta \quad (2.2)$$

for  $k \in \mathbb{N}$ . Thanks to the isomorphism between  $\mathbb{R}^2$  and  $\mathbb{C}$ , it is convenient to write  $m_k = c_k + is_k \in \mathbb{C}$  with  $i^2 = -1$ . We then see from Eq.(2.2) that

$$m_k = m_k(t, \mathbf{x}) = \int_{-\pi}^{\pi} f(t, \mathbf{x}, \theta) e^{ik\theta} d\theta \quad (2.3)$$

and hence  $m_{-k} = \overline{m_k}$  (the overline denotes the complex conjugate of a complex number). In this way, the governing equation for  $m_k$  can be deduced from Eq.(2.1) as

$$\partial_t m_k + v_0 \left( \frac{1}{2} \partial_x + \frac{1}{2i} \partial_y \right) m_{k+1} + v_0 \left( \frac{1}{2} \partial_x - \frac{1}{2i} \partial_y \right) m_{k-1} = \int_{-\pi}^{\pi} Q(f) e^{ik\theta} d\theta, \quad (2.4)$$

where the identities  $\cos \theta = (e^{i\theta} + e^{-i\theta})/2$ ,  $\sin \theta = (e^{i\theta} - e^{-i\theta})/2$  have been used. For the above equations, a finite truncation on  $k \leq N$  leaves (at least) the highest-order moment  $m_{N+1}$  being unclosed. This calls for a moment closure approach.

**2.1. Poisson-EQMOM.** We now propose a new extended quadrature method of moments equipped with the Poisson kernel (denoted Poisson-EQMOM). The key idea is to approximate the distribution  $f(\theta)$  with a convex combination of Poisson kernels:

$$f_N(\theta) = \sum_{\alpha=1}^N \rho_{\alpha} P_r(\phi_{\alpha} - \theta) \quad (2.5)$$

that matches the  $(N + 1)$  lower-order moments of  $f(\theta)$ :

$$m_k = \int_{-\pi}^{\pi} f_N(\theta) e^{ik\theta} d\theta = \sum_{\alpha=1}^N \rho_{\alpha} \int_{-\pi}^{\pi} e^{ik\theta} P_r(\phi_{\alpha} - \theta) d\theta \quad (2.6)$$

for  $k = 0, 1, \dots, N$ .

Obviously, such an ansatz introduces  $(2N + 1)$  unknowns collected as

$$W = (\rho_1, \dots, \rho_N, \phi_1, \dots, \phi_N, r)$$

to be solved by (2.6) from the transported moments  $m_0, \dots, m_N$  at each time  $t$  and position  $\mathbf{x}$ .

The Poisson kernel in (2.5) is defined for  $\theta \in [-\pi, \pi)$  and  $0 < r < 1$  as

$$P_r(\theta) = \frac{1}{2\pi} \frac{1 - r^2}{1 - 2r \cos \theta + r^2} = \frac{1}{2\pi} \sum_{k \in \mathbb{Z}} r^{|k|} e^{ik\theta}, \quad (2.7)$$

where the second expression gives the Fourier series of the Poisson kernel. It is seen in Fig. 1 that  $P_r(\theta)$  converges to a Dirac delta function centered at  $\theta = 0$  as  $r \rightarrow 1$ .

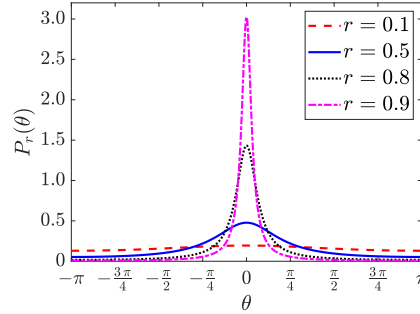


FIGURE 1. The Poisson kernels with different values of  $r$ .

The Poisson kernel has the following elegant property, which is the consequence of Theorems 5 and 15 in Section 2.2 of [12].

**Proposition 2.1.** *For any complex-valued function  $h(z)$  that is harmonic on  $\{z \in \mathbb{C} : |z| < 1\}$  and continuous on  $\{z \in \mathbb{C} : |z| \leq 1\}$ , we have*

$$h(re^{i\phi}) = \int_{-\pi}^{\pi} h(e^{i\theta}) P_r(\phi - \theta) d\theta.$$

In particular, this implies

$$r^k e^{ik\phi} = \int_{-\pi}^{\pi} e^{ik\theta} P_r(\phi - \theta) d\theta \quad (2.8)$$

for  $k = 0, 1, 2, \dots$ . Thus, Eq.(2.6) can be reformulated as

$$m_k = r^k \sum_{\alpha=1}^N \rho_{\alpha} e^{ik\phi_{\alpha}}, \quad k = 0, \dots, N, \quad (2.9)$$

or equivalently,

$$\begin{aligned} c_k &= r^k \sum_{\alpha=1}^N \rho_\alpha \cos k\phi_\alpha, \quad k = 0, 1, \dots, N, \\ s_k &= r^k \sum_{\alpha=1}^N \rho_\alpha \sin k\phi_\alpha, \quad k = 1, \dots, N. \end{aligned}$$

If  $W$  is solved from Eq.(2.9), then all the unclosed terms in Eq.(2.4) can be evaluated according to the Ansatz (2.5). For instance, the highest-order moment  $m_{N+1}$  is reconstructed as

$$\hat{m}_{N+1} = r^{N+1} \sum_{\alpha=1}^N \rho_\alpha e^{i(N+1)\phi_\alpha}. \quad (2.10)$$

As a consequence, we derive a closed moment system for  $\mathbf{M}_N = (m_0, \dots, m_N)^T \in \mathbb{C}^{N+1}$  which reads as

$$\partial_t \mathbf{M}_N + \frac{v_0}{2} \partial_x (F_1(\mathbf{M}_N) + F_2(\mathbf{M}_N)) + \frac{v_0}{2i} \partial_y (F_2(\mathbf{M}_N) - F_1(\mathbf{M}_N)) = S(\mathbf{M}_N) \quad (2.11)$$

with

$$F_1(\mathbf{M}_N) = (\overline{m_1}, m_0, \dots, m_{N-1})^T, \quad F_2(\mathbf{M}_N) = (m_1, \dots, m_N, \hat{m}_{N+1})^T,$$

and a model-specific source term  $S(\mathbf{M}_N) \in \mathbb{C}^{N+1}$ .

Clearly, solving the unknowns  $W$  from Eq.(2.9) plays a vital role in the Poisson-EQMOM. In the next subsection we show that such a  $W$  exists and the resultant approximation  $f_N = f_N(\theta)$  converges to  $f$  as  $N$  approaches infinity.

**2.2. Existence and convergence of  $f_N$ .** Denote  $\mathbb{T} = \{z \in \mathbb{C} : |z| = 1\}$  as the unit circle. Our main results in this subsection are stated as follows.

**Theorem 2.1.** *Assume that  $\mathbf{M}_N \in \mathbb{C}^{N+1}$  is realizable with respect to a certain measure  $\nu$  on  $\mathbb{T}$  (that is,  $m_k = \int_{\mathbb{T}} z^k d\nu(z)$  for  $k = 0, \dots, N$ ). Then there exists a unique  $r \in [0, 1]$  and the corresponding  $\rho_\alpha > 0$ ,  $\phi_\alpha \in [-\pi, \pi]$  ( $\alpha = 1, \dots, N$ ) solving Eq.(2.9), and any closure by the Poisson-EQMOM is well-defined.*

**Theorem 2.2.** *Assume that  $f(\theta) \geq c > 0$ . The following statements hold true.*

- (i). *If  $f$  is absolutely continuous and  $f' := df/d\theta \in L^2(-\pi, \pi)$ , then we have  $f_N \rightarrow f$  in  $L^2(-\pi, \pi)$  as  $N \rightarrow \infty$ .*
- (ii). *If  $f$  is Lipschitz, then we have  $f_N \rightarrow f$  in  $L^p(-\pi, \pi)$  for  $2 \leq p < \infty$ .*
- (iii). *If  $f$  is Lipschitz and  $f'$  is of bounded variation, then we have  $f_N \rightarrow f$  uniformly.*

*Remark 2.3.* Theorem 2.1 reveals that the Poisson-EQMOM enjoys a global property that all physically relevant moments are solvable. By contrast, for the 1-D velocity distribution, the Gaussian-EQMOM cannot be defined for certain moments generated with reasonable distributions (see Proposition 3.1 in [5]).

*Remark 2.4.* Theorem 2.2 demonstrates that the reconstructed distribution does converge to the original one if more moments are used, as long as the distribution has a positive lower bound. This property is definitely desired for any moment method, but seems not be verified for other kinds of quadrature-based method of moments.

The proof of Theorem 2.2 is quite technical and is therefore presented in Appendix A. In what follows we proceed to prove Theorem 2.1.

The main tool in our analysis is the Toeplitz matrix defined as [26]:

$$H_k = H_k(\mathbf{M}_N) = \begin{bmatrix} m_0 & m_1 & \cdots & m_k \\ \overline{m_1} & m_0 & \cdots & m_{k-1} \\ \vdots & \vdots & \ddots & \vdots \\ \overline{m_k} & \overline{m_{k-1}} & \cdots & m_0 \end{bmatrix} \in \mathbb{C}^{(k+1) \times (k+1)} \quad (2.12)$$

for  $k = 0, 1, \dots, N$ . The  $H_k$ 's are Hermitian matrices with real eigenvalues. We quote the following result, which is a consequence of Theorem 11.5, Proposition 11.15 and Proposition 11.16 of [26].

**Lemma 2.5.** *Given  $\mathbf{M}_N \in \mathbb{C}^{N+1}$ , the following two statements are equivalent.*

- (i). *The Toeplitz matrix  $H_N(\mathbf{M}_N)$  is positive semi-definite and its rank  $n$  is no larger than  $N$ .*
- (ii). *There exists an  $n$ -atomic measure  $\mu = \sum_{\alpha=1}^n \rho_\alpha \delta_{z_\alpha}$  on  $\mathbb{T}$  with  $\rho_\alpha > 0$  for all  $\alpha$  such that  $m_k = \int_{\mathbb{T}} z^k d\mu(z)$  for  $k = 0, \dots, N$ . Such a measure  $\mu$  is unique.*

As a first step, for  $r \in (0, 1]$ , Eq.(2.9) can be rewritten as

$$m_k r^{-k} = \int_{\mathbb{T}} z^k d\mu$$

with  $\mu = \sum_{\alpha=1}^n \rho_\alpha \delta_{z_\alpha}$  and  $z_\alpha = e^{i\phi_\alpha} \in \mathbb{T}$  for  $k = 0, \dots, N$ . According to Lemma 2.5, this requires the Toeplitz matrix corresponding to

$$\mathbf{M}_N^*(r) = (m_0, m_1 r^{-1}, \dots, m_N r^{-N}) \in \mathbb{C}^{N+1}, \quad (2.13)$$

denoted by  $H_N(\mathbf{M}_N^*(r))$ , to be positive semi-definite with  $\det H_N(\mathbf{M}_N^*(r)) = 0$ . In other words, the minimum eigenvalue of  $H_N(\mathbf{M}_N^*(r))$  must be zero.

Denote by  $\lambda(r; N)$  the minimum eigenvalue of  $H_N(\mathbf{M}_N^*(r))$ , which is a continuous function on  $r$ . We further show that

**Proposition 2.2.**  *$\lambda(r; N)$  is strictly increasing on  $r \in (0, 1]$ .*

*Proof.* For any  $0 < r_1 < r \leq 1$ , we denote  $\nu = \lambda(r_1; N)$  and  $\tilde{\mathbf{M}}_N = (\tilde{m}_0, \dots, \tilde{m}_N) \in \mathbb{C}^{N+1}$  with

$$\tilde{m}_0 = m_0 - \nu \geq 0 \text{ and } \tilde{m}_k = m_k \text{ for } k = 1, \dots, N.$$

It is straightforward to verify that

$$H_N(\tilde{\mathbf{M}}_N^*(r_1)) = H_N(\mathbf{M}_N^*(r_1)) - \nu I_{N+1}$$

with  $I_{N+1}$  being the unit matrix of order  $N+1$ , and hence the Toeplitz matrix  $H_N(\tilde{\mathbf{M}}_N^*(r_1))$  is positive semi-definite with zero determinant. According to Lemma 2.5, there exists a unique  $n$ -atomic measure  $\mu = \sum_{\alpha=1}^n \rho_\alpha \delta_{z_\alpha}$  for some  $n \leq N$  such that

$$\tilde{m}_k r_1^{-k} = \int_{\mathbb{T}} z^k d\mu(z) = \sum_{\alpha=1}^n \rho_\alpha z_\alpha^k$$

holds for  $k = 0, \dots, N$ . Writing  $z_\alpha = e^{i\phi_\alpha}$ , we obtain

$$\tilde{m}_k r^{-k} = (r_1/r)^k \sum_{\alpha=1}^n \rho_\alpha e^{ik\phi_\alpha} = \sum_{\alpha=1}^n \rho_\alpha \int_{-\pi}^{\pi} e^{ik\theta} P_{r_1/r}(\phi_\alpha - \theta) d\theta, \quad (2.14)$$

where the second equality results from Eq.(2.8).

Now we claim that the Toeplitz matrix  $H_N(\tilde{\mathbf{M}}_N^*(r))$  is positive definite. To see this, take any nonzero  $a = (a_0, \dots, a_N)^T \in \mathbb{C}^{N+1}$  and compute

$$\begin{aligned} \bar{a}^T H_N(\tilde{\mathbf{M}}_N^*(r)) a &= \sum_{k,l=0}^N \bar{a}_k a_l \tilde{m}_{l-k} r^{-|l-k|} \\ &= \sum_{\alpha=1}^n \rho_\alpha \int_{-\pi}^{\pi} \left[ \sum_{k,l=0}^N \bar{a}_k a_l e^{i(l-k)\theta} \right] P_{r_1/r}(\phi_\alpha - \theta) d\theta \\ &= \sum_{\alpha=1}^n \rho_\alpha \int_{-\pi}^{\pi} \left| \sum_{l=0}^N a_l e^{il\theta} \right|^2 P_{r_1/r}(\phi_\alpha - \theta) d\theta > 0. \end{aligned}$$

Here we have used Eq.(2.14) to obtain the second equality. Note that for  $l < k$ , Eq.(2.14) should be used with the complex conjugate taken on the both sides.

Therefore, the minimum eigenvalue of  $H_N(\tilde{\mathbf{M}}_N^*(r))$  is strictly positive. Further noticing

$$H_N(\tilde{\mathbf{M}}_N^*(r)) = H_N(\mathbf{M}_N^*(r)) - \nu I_{N+1},$$

we conclude  $\lambda(r; N) > \nu = \lambda(r_1; N)$ , which completes the proof.  $\square$

The following fact will also be needed.

**Proposition 2.3.** *Suppose that  $\nu$  is a measure on  $\mathbb{T}$  with at least  $(N+1)$  points of support. If  $m_k = \int z^k d\nu$  for  $k = 0, \dots, N$ , then the Toeplitz matrix  $H_N(\mathbf{M}_N^*(1)) = H_N(\mathbf{M}_N)$  is positive definite*

*Proof.* For any nonzero  $a = (a_0, \dots, a_N)^T \in \mathbb{C}^{N+1}$ , we define a polynomial  $p(z) = \sum_{j=0}^N a_j z^j$  and compute

$$\bar{a}^T H_N(\mathbf{M}_N^*(1)) a = \sum_{j,k=0}^N \bar{a}_j a_k m_{k-j} = \int \sum_{j,k=0}^N \bar{a}_j a_k z^{k-j} d\nu = \int |p(z)|^2 d\nu.$$

Since there exists  $z_0 \in \text{supp } \nu$  such that  $p(z_0) \neq 0$ , we have  $\int |p(z)|^2 d\nu > 0$  and hence  $H_N(\mathbf{M}_N^*(1))$  is positive definite.  $\square$

With these preparations at hand, we are ready to prove Theorem 2.1.

*Proof of Theorem 2.1.* If the measure  $\nu$  has no more than  $N$  points of support, clearly  $r = 1$  is a solution to Eq.(2.9) with  $\det H_N(\mathbf{M}_N^*(1)) = 0$ . The solution is unique because for any  $r' < 1$ , we see from Proposition 2.2 that  $\lambda(r'; N) < 0$  and hence no measure can generate  $\mathbf{M}_N^*(r')$ , as illustrated in Lemma 2.5.

Now suppose that  $\nu$  has at least  $(N+1)$  points of support. If  $m_1 = \dots = m_N = 0$ , it can be verified that  $r = 0$ ,  $\sum_{\alpha} \rho_{\alpha} = m_0$  and arbitrary  $\phi_{\alpha}$  constitute a solution to Eq.(2.9). On the other hand, for any  $r' > 0$ , the equations  $\sum_{\alpha} \rho_{\alpha} z_{\alpha}^k = 0$  with  $|z_{\alpha}| = 1$  for  $k = 1, \dots, N$  can only lead to  $\rho_{\alpha} = 0$  for all  $\alpha$ , a contradiction to  $m_0 > 0$ . Thus,  $r = 0$  is the only solution in this case.

If  $(m_1, \dots, m_N) \neq \mathbf{0}$ , then we claim

$$\lim_{r \rightarrow 0^+} \lambda(r; N) < 0.$$

To see this, let  $k$  be that  $m_1 = \dots = m_{k-1} = 0$  and  $m_k \neq 0$ . Then the determinant

$$\det(H_k(\mathbf{M}_N^*(r))) = \det \begin{bmatrix} m_0 & 0 & \dots & 0 & m_k r^{-k} \\ & m_0 & & & \\ & & \ddots & & \\ & & & m_0 & \\ \overline{m_k} r^{-k} & 0 & \dots & 0 & m_0 \end{bmatrix}$$

has a leading term  $-m_0^{k-1} |m_k|^2 r^{-2k}$  and hence goes to  $-\infty$  as  $r \rightarrow 0^+$ . This implies that  $H_k(\mathbf{M}_N^*(r))$  has negative eigenvalues as  $r \rightarrow 0^+$ . Our claim thus follows because the minimum eigenvalue of  $H_N(\mathbf{M}_N^*(r))$  can never be greater than that of its principal minor. Since  $\lambda(r; N)$  is strictly increasing on  $r \in (0, 1]$  (Proposition 2.2) and  $\lambda(1; N) > 0$  (Proposition 2.3), it becomes clear that there exists a unique  $r \in (0, 1)$ , together with a corresponding  $n$ -atomic measure  $\mu = \sum_{\alpha} \rho_{\alpha} \delta_{z_{\alpha}}$  on  $\mathbb{T}$  with  $n \leq N$ , that solves Eq.(2.9).

In all three cases, it is straightforward to show that the unclosed terms (for instance,  $m_{N+1}$ ) can be uniquely determined from  $m_0, \dots, m_N$ . Thus, the Poisson-EQMOM is well-defined.  $\square$

### 3. MOMENT INVERSION ALGORITHM

Our analysis in the previous section not only reveals the nice property of the Poisson-EQMOM, but also gives clue to a practical algorithm solving Eq.(2.9). Generally, given any realizable moment  $\mathbf{M}_N$ , the algorithm consists of the following three steps:

- (i) Find  $r \in [0, 1]$ , which will be detailed in Section 3.1;
- (ii) Solve  $\phi_1, \dots, \phi_N$ , as presented in Section 3.2;

(iii) Solve  $\rho_1, \dots, \rho_N$  from the linear equation

$$\begin{bmatrix} 1 & 1 & \cdots & 1 \\ z_1 & z_2 & \cdots & z_N \\ \vdots & \vdots & & \vdots \\ z_1^{N-1} & z_2^{N-1} & \cdots & z_N^{N-1} \end{bmatrix} \begin{bmatrix} \rho_1 \\ \rho_2 \\ \vdots \\ \rho_N \end{bmatrix} = \begin{bmatrix} m_0 \\ m_1 \\ \vdots \\ m_{N-1} \end{bmatrix}. \quad (3.1)$$

Here we denote  $z_\alpha = e^{i\phi_\alpha}$  for  $\alpha = 1, \dots, N$ . In practice,  $\rho_\alpha$  can be solved from the real part of the above equation, that is,  $\sum_{\alpha=1}^N \rho_\alpha \cos k\phi_\alpha = c_k$  for  $k = 0, 1, \dots, N-1$ .

**3.1. Locating  $r$ .** Two approaches are available for this purpose. The more effective strategy is to numerically compute the minimum eigenvalue of  $H_N(M_N^*(r))$ , which is expected to be zero for the desired  $r$ . As the minimum eigenvalue increases monotonically on  $r \in [0, 1]$ , a simple bisection algorithm on the interval  $[0, 1]$  can be applied to locate  $r$ . In each iteration step, the minimum eigenvalue is computed by the MATLAB function `eig` [20].

On the other hand,  $r$  can also be determined with a  $t$ -polynomial

$$p_N(t) := \det H_N(M_N^*(1/t))$$

of degree  $\frac{N^2+2N+\text{mod}(N,2)}{2}$ . Let  $t_m$  be the smallest root of  $p_N$  on the interval  $[1, \infty]$ . Then we have  $r = t_m^{-1}$ , corresponding to the greatest root of  $\det H_N(M_N^*(r))$  on  $r \in [0, 1]$ . To see this, just notice that for any smaller root  $r'$  (if ever exists),  $H_N(M_N^*(r'))$  must have negative eigenvalues, as indicated by Proposition 2.2. Consequently, according to Lemma 2.5, there is no measure with exactly  $N$  points of support that generates  $M_N^*(r')$ .

The polynomials  $p_N(t)$  can be explicitly computed for small values of  $N$ :

$$\begin{aligned} p_1(t) &= m_0^2 - |m_1|^2 t^2, \\ p_2(t) &= m_0^3 - 2m_0|m_1|^2 t^2 + [2\Re(\overline{m_1}^2 m_2) - m_0|m_2|^2] t^4, \\ p_3(t) &= m_0^4 - 3m_0^2|m_1|^2 t^2 + [4\Re(m_0\overline{m_1}^2 m_2) - 2m_0^2|m_2|^2 + |m_1|^4] t^4 \\ &\quad + [4\Re(m_0\overline{m_1}m_2 m_3) - 2\Re(\overline{m_1}^3 m_3) - m_0^2|m_3|^2 - 2|m_1 m_2|^2] t^6 \\ &\quad + [|m_2|^4 + |m_1 m_3|^2 - 2\Re(\overline{m_1} m_2^2 \overline{m_3})] t^8, \end{aligned}$$

with  $\Re(z)$  denoting the real part of  $z \in \mathbb{C}$ . Thus, the smallest root  $t_m$  on  $[1, \infty]$  can be found by existing algorithms. However, as  $N$  grows larger, the explicit forms of  $p_N(t)$  will soon become intractable.

**3.2. Solving  $\phi_\alpha$ 's.** The key idea to solve the  $\phi_\alpha$ 's is to seek the roots of orthogonal polynomials. Given a moment set  $\mathbf{M}_N \in \mathbb{C}^{N+1}$ , assume that the Toeplitz matrix  $H_N(\mathbf{M}_N)$  is positive semi-definite with its rank being  $n \leq N$ . Define  $P_0(z) = 1$  and

$$P_k(z) = \frac{1}{\det H_{k-1}} \det \begin{bmatrix} m_0 & m_1 & \cdots & m_{k-1} & m_k \\ \overline{m_1} & m_0 & \cdots & m_{k-2} & m_{k-1} \\ \vdots & \vdots & & \vdots & \vdots \\ \overline{m_{k-1}} & \overline{m_{k-2}} & \cdots & m_0 & m_1 \\ 1 & z & \cdots & z^{k-1} & z^k \end{bmatrix} \quad (3.2)$$

for  $k = 1, \dots, n$ . These are monic polynomials of degree  $k$ .

To see the 'orthogonality', we introduce a sesquilinear form  $\langle \cdot, \cdot \rangle$  on the polynomial space  $\mathbb{C}[z]_n$  as

$$\langle z^j, z^k \rangle = m_{k-j}, \quad j, k = 0, 1, \dots, n. \quad (3.3)$$

This is actually a complex Hermitian form due to our convention  $m_{-k} = \overline{m_k}$ . It is not difficult to verify that

$$\langle P_k(z), z^j \rangle = \frac{1}{\det H_{k-1}} \det \begin{bmatrix} m_0 & \overline{m_1} & \cdots & \overline{m_{k-1}} & \overline{m_k} \\ m_1 & m_0 & \cdots & \overline{m_{k-2}} & \overline{m_{k-1}} \\ \vdots & \vdots & & \vdots & \vdots \\ m_{k-1} & m_{k-2} & \cdots & m_0 & \overline{m_1} \\ m_j & m_{j-1} & \cdots & m_{j-k+1} & m_{j-k} \end{bmatrix} = \frac{\det H_k}{\det H_{k-1}} \delta_{jk}$$

for  $j = 0, 1, \dots, k$ . Here  $\delta_{jk}$  denotes the Kronecker delta. Obviously, this implies

$$\langle P_k(z), P_j(z) \rangle = \frac{\det H_k}{\det H_{k-1}} \delta_{jk} \quad \text{and} \quad \langle P_n(z), P_n(z) \rangle = 0.$$

Another ingredient we need is the recursive formula of the orthogonal polynomials. Define  $P_0^*(z) = 1$  and

$$P_k^*(z) = \frac{1}{\det H_{k-1}} \det \begin{bmatrix} m_0 & \overline{m_1} & \cdots & \overline{m_{k-1}} & \overline{m_k} \\ m_1 & m_0 & \cdots & \overline{m_{k-2}} & \overline{m_{k-1}} \\ \vdots & \vdots & & \vdots & \vdots \\ m_{k-1} & m_{k-2} & \cdots & m_0 & \overline{m_1} \\ z^k & z^{k-1} & \cdots & z & 1 \end{bmatrix}$$

for  $k = 1, \dots, n$ . Similarly, one can check that

$$\langle P_k^*(z), z^j \rangle = \frac{\det H_k}{\det H_{k-1}} \delta_{0j}$$

for  $j = 0, 1, \dots, k$ . Then the following relations hold [26]:

$$P_{k+1}(z) = zP_k(z) - \overline{a_k}P_k^*(z), \quad P_{k+1}^*(z) = P_k^*(z) - a_k zP_k(z) \quad (3.4)$$

for  $k = 0, 1, \dots, n-1$  with

$$a_k = -\overline{P_{k+1}(0)} = \frac{\det H_{k-1}}{\det H_k} \langle zP_k, 1 \rangle.$$

Now let us specify the arbitrary moment set  $\mathbf{M}_N$  to be  $\mathbf{M}_N^*(r)$  in Eq.(2.13), so obviously our assumption on the Toeplitz matrix  $H_N(\mathbf{M}_N^*(r))$  holds true. If the polynomials  $P_k(z)$  in Eq.(3.2) and the Hermitian form in Eq.(3.3) are both defined based on  $\mathbf{M}_N^*(r)$ , then we claim that

**Proposition 3.1.** *The roots of  $P_n(z)$  are just  $z_\alpha = e^{i\phi_\alpha}$  for  $\alpha = 1, \dots, n$ .*

*Proof.* Denote  $m_k^* = m_k r^{-k}$ . According to Lemma 2.5, there exists a unique  $n$ -atomic measure  $\mu = \sum_{\alpha=1}^n \rho_\alpha \delta_{z_\alpha}$  on  $\mathbb{T}$  such that  $m_k^* = \int z^k d\mu$ , where  $z_\alpha = e^{i\phi_\alpha}$  are just what we need. Then the Hermitian form Eq.(3.3) is rewritten as  $\langle z^j, z^k \rangle = m_{k-j}^* = \int z^{k-j} d\mu$ . It is straightforward to verify that for any  $p, q \in \mathbb{C}[z]_n$ , we have

$$\langle p, q \rangle = \int \bar{p} q d\mu.$$

In particular, it is seen that

$$\langle P_n(z), P_n(z) \rangle = \int |P_n(z)|^2 d\mu = 0,$$

which implies  $P(z_\alpha) = 0$  for all  $\alpha$ . □

For convenience, define  $Q_0(z) = 1$  and  $Q_k(z) = \sqrt{\det H_{k-1} / \det H_k} P_k(z)$  for  $k = 1, \dots, n-1$ . Clearly, we have  $\langle Q_k(z), Q_j(z) \rangle = \delta_{kj}$ , indicating that  $\{Q_k\}_{k=0}^{n-1}$  is the (unique) orthonormal base of  $\mathbb{C}[z]_{n-1}$ . As a consequence, we can express  $zQ_k(z)$  as

$$zQ_k(z) = \sum_{j=0}^{k+1} a_{kj} Q_j(z)$$



for  $k = 0, 1, \dots, n-2$ . A similar relation for  $zQ_{n-1}(z)$  can be obtained from Eq.(3.4) as

$$zQ_{n-1}(z) = \sum_{j=0}^{n-1} a_{n-1,j} Q_j(z) + \sqrt{\frac{\det H_{n-2}}{\det H_{n-1}}} P_n(z),$$

because  $P_{n-1}^*(z)$  can also be linearly generated by  $\{Q_k\}_{k=0}^{n-1}$ . The last two relations can be concisely organized as

$$z \begin{bmatrix} Q_0(z) \\ \vdots \\ Q_{n-2}(z) \\ Q_{n-1}(z) \end{bmatrix} = \mathbf{J} \begin{bmatrix} Q_0(z) \\ \vdots \\ Q_{n-2}(z) \\ Q_{n-1}(z) \end{bmatrix} + \begin{bmatrix} 0 \\ \vdots \\ 0 \\ \sqrt{\frac{\det H_{n-2}}{\det H_{n-1}}} P_n(z) \end{bmatrix}$$

with  $\mathbf{J} = (a_{kj}) \in \mathbb{C}^{(n+1) \times (n+1)}$  and  $a_{kj} = 0$  for  $j \geq k+2$ . It thus becomes clear that the roots of  $P_n(z)$  are the eigenvalues of  $\mathbf{J}$ .

The elements of  $\mathbf{J}$  can be computed iteratively. If  $Q_k(z)$  is already known, then we have

$$a_{kj} = \langle zQ_k(z), Q_j(z) \rangle \quad \text{for } j = 0, \dots, k. \quad (3.5)$$

Compute

$$R_{k+1}(z) = zQ_k(z) - \sum_{j=0}^k a_{kj} Q_j(z), \quad (3.6)$$

which has a degree  $k+1$  and is orthogonal to  $Q_j(z)$  for  $j = 0, \dots, k$ . Therefore,  $Q_{k+1}(z)$  can be obtained via

$$a_{k,k+1} = \sqrt{\langle R_{k+1}(z), R_{k+1}(z) \rangle}, \quad (3.7)$$

$$Q_{k+1}(z) = \frac{R_{k+1}(z)}{a_{k,k+1}}. \quad (3.8)$$

This gives a practical algorithm for solving the  $\phi_\alpha$ 's with a given moment set  $M_N^*(r)$ .

*Remark 3.1.* For the degenerated case with  $n = \text{rank } M_N^*(r) < N$ , only  $n$  nodes  $z_\alpha = e^{i\phi_\alpha}$  ( $\alpha = 1, \dots, n$ ) can be solved from the above procedure, and the rest nodes can be chosen arbitrarily with zero weights.

**3.3. Lifting  $m_0$ .** Two issues remain for the moment inversion process presented in the previous subsections. First, it may be computationally costly to solve  $r$  iteratively as in subsection 3.1. Second, the approximation  $f_N$  may deviate significantly from the ‘correct’ distribution  $f$  especially when the number of nodes  $N$  is not too large. The latter is clearly illustrated in Fig. 2, where the original von Mises distribution reads as

$$f_{vM}(\theta) = C \exp\left(\frac{\cos \theta}{d}\right)$$

with  $C$  being a scaling factor such that  $\int_{-\pi}^{\pi} f_{vM} d\theta = 1$ . As seen in Fig. 2a, if  $d = 0.8$  (corresponding to a ‘wide’ distribution), the 8-node Poisson-EQMOM (with  $\ell = 0$ ) generates a reasonable approximation to  $f_{vM}$ . In contrast, for the ‘narrower’ distribution with  $d = 0.4$ , the 8-node reconstruction is very different from the von Mises distribution; see Fig. 2b and the large  $L^2$ -error in Fig. 2d for  $\ell = 0$ . While simply increasing the number of nodes does imply a trend for  $f_N$  to be closer to  $f_{vM}$ , there remains a non-negligible error even when  $N$  reaches 32. This poses challenges to solving the moment closure system (2.11) as the closed moment  $\hat{m}_{N+1}$  may become inaccurate, as demonstrated in Table 1 for the von Mises case with  $d = 0.4$ .

Inspired by the condition in Theorem 2.2 (that  $f$  has a positive lower bound), we propose a remedy, which is simply raising  $m_0$  by some quantity  $\ell$  (with other moments unchanged) before performing moment inversion. This is equivalent to inverting the moments generated by  $f(\theta) + \ell$  because the constant function on  $\mathbb{T}$  has zero moments  $m_k = 0$  for  $k \geq 1$ . With the lifted moments  $(m_0 + \ell, m_1, \dots, m_N)$ , the

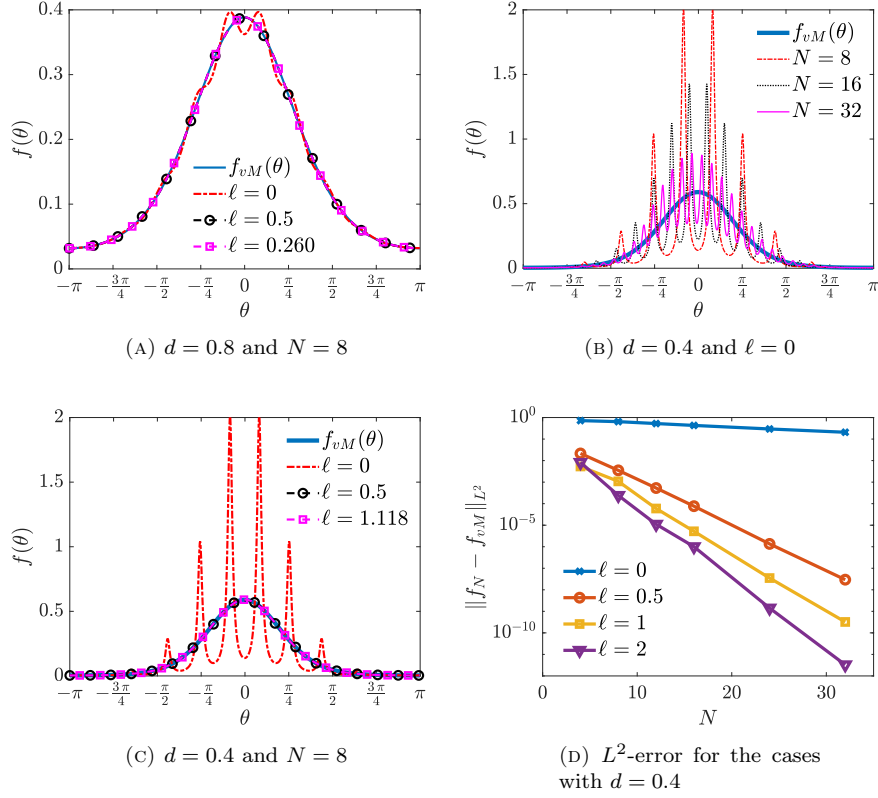


FIGURE 2. Reconstruction of the von Mises distribution by the Poisson-EQMOM.

TABLE 1.  $|\hat{m}_{N+1} - m_{N+1}|$  for the von Mises distribution with  $d = 0.4$ 

$N$	$\ell = 0$	$\ell = 0.5$	$\ell = 1$	$\ell = 2$
4	0.1154	0.01698	0.005697	0.01389
8	0.09176	0.001776	0.001535	$3.694 \times 10^{-4}$
12	0.07687	$1.599 \times 10^{-4}$	$1.011 \times 10^{-6}$	$3.685 \times 10^{-6}$
16	0.06484	$8.005 \times 10^{-6}$	$8.880 \times 10^{-6}$	$1.727 \times 10^{-6}$
24	0.04627	$6.069 \times 10^{-7}$	$4.172 \times 10^{-8}$	$7.589 \times 10^{-10}$
32	0.04420	$3.727 \times 10^{-8}$	$1.018 \times 10^{-10}$	$4.056 \times 10^{-12}$

inverted parameters are denoted as  $(\rho_\alpha^{(\ell)}, \phi_\alpha^{(\ell)}, r^{(\ell)})_{\alpha=1}^N$ , all relying on  $\ell$ . The Poisson-EQMOM ansatz Eq.(2.5) now becomes

$$f_{N,\ell}(\theta) = \sum_{\alpha=1}^N \rho_\alpha^{(\ell)} P_{r^{(\ell)}}(\phi_\alpha^{(\ell)} - \theta) - \ell \quad (3.9)$$

for moment closure. In particular,  $\hat{m}_{N+1}$  has the same form as Eq.(2.10).

It is seen from Figs. 2a&c that with certain values of lift-up  $\ell$ , the recovered  $f_{N,\ell}$ 's are much more precise especially for the case with  $d = 0.4$ . The improvement is more clearly manifested in Fig. 2d and Table 1: with the presence of lift-up, the  $L^2$ -error is reduced by several orders for a fixed  $N$ , and can be more effectively eliminated by adding  $N$  as compared with the zero lift-up cases. Such an observation is consistent with the pointwise convergence of  $f_N$  to  $f$  in Theorem 2.2. Therefore, we believe that lifting  $m_0$  is an indispensable part of the moment inversion process.

In the practical simulation, the flexible choice of  $\ell$  makes it possible to accelerate the calculation of  $r$ . Given  $\mathbf{M}_N = (m_0, \dots, m_N) \in \mathbb{C}^{N+1}$ , we set  $r_1 = |m_1|/m_0$  and the eigenvalues of  $H_1(\mathbf{M}_N^*(r_1)) = \begin{bmatrix} m_0 & m_1/r_1 \\ \bar{m}_1/r_1 & m_0 \end{bmatrix}$  are 0 and  $2m_0$ . Thus, the minimum eigenvalue  $\lambda(r_1; N)$  must be non-positive, and we just take  $\ell = |\lambda(r_1; N)|$ . It is easy to see that for  $\mathbf{M}_{N\ell} = (m_0 + \ell, m_1, \dots, m_N)$ , the minimum eigenvalue of  $H_N(\mathbf{M}_{N\ell}^*(r_1))$  is zero, so the remaining task is to solve  $\phi_\alpha$  and  $\rho_\alpha$  based on  $\mathbf{M}_{N\ell}^*(r_1)$ . Clearly, this approach computes the minimum eigenvalue of a matrix only once. The performance is first examined in Figs. 2a (the case  $\ell = 0.260$ ) and c (the case  $\ell = 1.118$ ). Moreover, such a choice of  $\ell$  is applied in our numerical tests in Section 6 and always yields satisfactory results therein.

Table 2 presents a summary on the moment inversion algorithm. For a realizable moment set, the procedure is shown to be robust against the increment of  $N$  which can go up to 100.

TABLE 2. A summary on the moment inversion algorithm

Step 0	Given $\mathbf{M}_N = (m_0, \dots, m_N) \in \mathbb{C}^{N+1}$ .
Step 1	Compute $r =  m_1 /m_0$ and $\ell = -\lambda(r; N) \geq 0$ .
Step 2	$\mathbf{M}_N \leftarrow (m_0 + \ell, \frac{m_1}{r}, \dots, \frac{m_N}{r})$ .
Step 3	Define the Hermitian form $\langle z^j, z^k \rangle = m_{k-j}$ .
Step 4	Compute the elements of $\mathbf{J}$ iteratively by Eqs.(3.5)-(3.8).
Step 5	Solve $z_\alpha = e^{i\phi_\alpha}$ ( $\alpha = 1, \dots, N$ ) as the eigenvalues of $\mathbf{J}$ .
Step 6	Solve $\rho_\alpha$ ( $\alpha = 1, \dots, N$ ) by Eq.(3.1).

#### 4. APPLICATION TO POLAR ACTIVE FLOWS

We now apply the Poisson-EQMOM to a 2D kinetic equation associated with the celebrated Vicsek model [28]. The evolution of  $f = f(t, \mathbf{x}, \theta)$  is governed by [9]

$$\epsilon(\partial_t f + \mathbf{e}_\theta \cdot \nabla_{\mathbf{x}} f) = Q(f) := \mathbf{d} \partial_\theta^2 f + \nu \partial_\theta ((\Omega \times \mathbf{e}_\theta) f). \quad (4.1)$$

In the Vicsek dynamics, each polar active particle continuously adjusts its velocity direction to the neighboring mean velocity direction

$$\Omega = \Omega[f](t, \mathbf{x}) = \frac{j[f](t, \mathbf{x})}{|j[f](t, \mathbf{x})|} \in S^1 \quad \text{with } j[f](t, \mathbf{x}) = \int_{-\pi}^{\pi} \mathbf{e}_\theta f(\theta) d\theta. \quad (4.2)$$

Writing  $\Omega = (\Omega_x, \Omega_y) = (\cos \bar{\theta}, \sin \bar{\theta})$ , we see that the cross product

$$\Omega \times \mathbf{e}_\theta = \Omega_x \sin \theta - \Omega_y \cos \theta = \sin(\theta - \bar{\theta})$$

quantifies the angle between the single particle velocity  $\mathbf{e}_\theta$  and the neighboring mean direction  $\Omega$ .  $\nu > 0$  is the constant intensity of velocity alignment. But the alignment is not perfect. The competing mechanism is the Gaussian (or uniform) noise on  $[-\pi, \pi]$ , with  $\mathbf{d} > 0$  characterizing the noise strength. The whole system can be rescaled and produces a scaling parameter  $\epsilon$  as the ratio between micro and macro variables. The hydrodynamic limit is derived with  $\epsilon \rightarrow 0$ .

As a remarkable feature of Eq.(4.1), the collision operator  $Q(f)$  can be rewritten as [9]

$$Q(f) = \frac{\mathbf{d}}{\nu} \partial_\theta \left( M_{\bar{\theta}} \partial_\theta \left( \frac{f}{M_{\bar{\theta}}} \right) \right)$$

with  $M_{\bar{\theta}} = M_{\bar{\theta}}(\theta)$  being the von Mises distribution:

$$M_{\bar{\theta}}(\theta) = C \exp \left( \frac{\nu \cos(\theta - \bar{\theta})}{\mathbf{d}} \right). \quad (4.3)$$

It holds true that

$$H(f) := \int_{-\pi}^{\pi} Q(f) \frac{f}{M_{\bar{\theta}}} d\theta = - \int_{-\pi}^{\pi} M_{\bar{\theta}} \partial_\theta^2 \left( \frac{f}{M_{\bar{\theta}}} \right) d\theta \leq 0.$$

Therefore, the equilibrium that vanishes  $Q(f)$  can only be von Mises distributions.

The moment system derived from the  $N$ -node Poisson-EQMOM has the form of Eq.(2.11) (with  $v_0 = 1$  and  $\epsilon$  included). The source term  $S(\mathbf{M}_N) = (q_0, q_1, \dots, q_N)$  can now be determined by a direct calculation:

$$q_k := \int_{-\pi}^{\pi} e^{ik\theta} Q(f) d\theta = \mathbf{d} \int_{-\pi}^{\pi} e^{ik\theta} \partial_{\theta}^2 f d\theta + \nu \int_{-\pi}^{\pi} e^{ik\theta} \partial_{\theta} ((\Omega \times \mathbf{e}_{\theta}) f) d\theta.$$

Using the integration by parts gives

$$\int_{-\pi}^{\pi} e^{ik\theta} \partial_{\theta}^2 f d\theta = (ik)^2 \int_{-\pi}^{\pi} f e^{ik\theta} d\theta = -k^2 m_k$$

and

$$\begin{aligned} \int_{-\pi}^{\pi} e^{ik\theta} \partial_{\theta} ((\Omega \times \mathbf{e}_{\theta}) f) d\theta &= -ik \int_{-\pi}^{\pi} e^{ik\theta} (\Omega_x \sin \theta - \Omega_y \cos \theta) f d\theta \\ &= -ik \left[ \frac{\Omega_x}{2i} (m_{k+1} - m_{k-1}) - \frac{\Omega_y}{2} (m_{k+1} + m_{k-1}) \right] \\ &= \frac{k}{2} [(\Omega_x + i\Omega_y) m_{k-1} - (\Omega_x - i\Omega_y) m_{k+1}] \\ &= \frac{k}{2|m_1|} (m_1 m_{k-1} - \overline{m_1} m_{k+1}). \end{aligned}$$

Here we have used the identity  $\Omega_x + i\Omega_y = m_1/|m_1|$ , which can be easily seen from Eq.(4.2). Therefore, the source term  $S(\mathbf{M}_N)$  is obtained with

$$q_k = -\mathbf{d} k^2 m_k + \mathbf{1}_{|m_1|>0} \cdot \frac{\nu k}{2|m_1|} (m_1 m_{k-1} - \overline{m_1} m_{k+1}) \quad (4.4)$$

for  $k = 0, \dots, N$ . Clearly, no other term except for  $m_{N+1}$  needs to be closed, and  $q_0 = 0$  indicates that the system respects mass conservation.

**4.1. Hyperbolicity with  $N = 1$ .** We briefly discuss the hyperbolicity of the resultant moment system as first-order PDEs. For the single-node system, the unknown is  $\mathbf{c} = (c_0, c_1, s_1)^T$ , and the closure is performed such that  $\rho_1 = m_0$ ,  $r = |m_1|/m_0$ ,  $e^{i\phi_1} = m_1/|m_1|$  and hence

$$m_2 = r^2 \rho_1 e^{2i\phi_1} = \frac{m_1^2}{m_0} \Leftrightarrow c_2 = \frac{c_1^2 - s_1^2}{c_0}, \quad s_2 = \frac{2c_1 s_1}{c_0}.$$

The resultant moment system is explicitly presented as

$$\partial \mathbf{c} + A_x \partial_x \mathbf{c} + A_y \partial_y \mathbf{c} = \frac{1}{\epsilon} (0, \Re(q_1), \Im(q_1))^T \quad (4.5)$$

with

$$A_x = \begin{bmatrix} 0 & 1 & 0 \\ \frac{1}{2} - \frac{c_1^2 - s_1^2}{2c_0^2} & \frac{c_1}{c_0} & -\frac{s_1}{c_0} \\ -\frac{c_1 s_1}{c_0^2} & \frac{s_1}{c_0} & \frac{c_1}{c_0} \end{bmatrix}, \quad A_y = \begin{bmatrix} 0 & 0 & 1 \\ -\frac{c_1 s_1}{c_0^2} & \frac{s_1}{c_0} & \frac{c_1}{c_0} \\ \frac{1}{2} + \frac{c_1^2 - s_1^2}{2c_0^2} & -\frac{c_1}{c_0} & \frac{s_1}{c_0} \end{bmatrix}$$

and

$$\begin{aligned} \Re(q_1) &= -\mathbf{d} c_1 + \mathbf{1}_{|m_1|>0} \cdot \frac{\nu}{2|m_1|} (c_0 c_1 - c_1 c_2 - s_1 s_2), \\ \Im(q_1) &= -\mathbf{d} s_1 + \mathbf{1}_{|m_1|>0} \cdot \frac{\nu}{2|m_1|} (c_0 s_1 - c_1 s_2 + s_1 c_2) \end{aligned}$$

being the real and imaginary parts of  $q_1$ , respectively. Our result is stated as follows.

**Proposition 4.1.** *The moment system (4.5) is strictly hyperbolic if  $0 \leq r < 1$ .*

*Proof.* For any  $a, b \in \mathbb{R}$  with  $a^2 + b^2 > 0$ , the characteristic polynomial  $p(\lambda)$  of  $aA_x + bA_y$  can be derived through a straightforward calculation as

$$p(\lambda) = \left( \lambda - \frac{ac_1 + bs_1}{c_0} \right) \left( \lambda^2 - \frac{ac_1 + bs_1}{c_0} \lambda - \frac{a^2 + b^2}{2} (1 - r^2) \right),$$

where we have used the relation  $r^2 = (c_1^2 + s_1^2)/c_0^2$ . Since  $(a^2 + b^2)(1 - r^2) > 0$ , it is not difficult to verify that  $p(\lambda)$  has three distinct real roots.  $\square$

*Remark 4.1.* If  $r = 1$ ,  $f$  has a single support  $f(\theta) = c_0\delta(\theta - \theta_0)$  (see the proof of Theorem 2.1), implying  $c_1 = c_0 \cos \theta_0$  and  $s_1 = c_0 \sin \theta_0$ . In this case, the system (4.5) is not hyperbolic.

To see this, just take  $a = 1$ ,  $b = 0$  and notice from the expression of  $p(\lambda)$  that  $c_1/c_0 = \cos \theta_0$  is an eigenvalue of  $A_x$  with the algebraic multiplicity 2. Then the corresponding eigenvector  $u = (u_1, u_2, u_3) \in \mathbb{R}^3$  can be solved from  $A_x u = u \cos \theta_0$ , yielding  $u_2 = u_1 \cos \theta_0$  and  $u_3 = u_1 \sin \theta_0$  (if  $\sin \theta_0 \neq 0$ ). This shows that the eigenvalue  $\cos \theta_0$  has the geometric multiplicity 1, and hence  $A_x$  is not diagonalizable if  $\sin \theta_0 \neq 0$ . But the case  $\sin \theta_0 = 0$  (that is,  $s_1 = 0$  and  $c_1 = c_0$ ) simply renders  $A_y$  not diagonalizable.

The non-hyperbolicity with the use of delta functions for moment closure, a method sometimes termed the quadrature method of moments (QMOM), has also been observed in the treatment of Boltzmann-like equations [6, 15]. The hyperbolicity of the multiple-node Poisson-EQMOM is left for future work.

## 5. NUMERICAL SCHEME

The numerical scheme for the moment closure system involves a splitting method which solves separately

$$\partial_t m_k + \frac{v_0}{2} \partial_x (m_{k+1} + m_{k-1}) + \frac{v_0}{2i} \partial_y (m_{k+1} - m_{k-1}) = 0, \quad (5.1)$$

$$\partial_t m_k = \frac{1}{\epsilon} q_k(\mathbf{M}_N) \quad (5.2)$$

for  $k = 0, \dots, N$ .

**5.1. Transport and kinetic-based flux.** Eq.(5.1) is treated with the first-order schemes (to simplify the notation, only the spatial 1D case is illustrated here):

$$\frac{m_{k,j}^* - m_{k,j}^n}{\Delta t} + \frac{v_0}{2} \frac{\mathcal{F}_{k+1,j+\frac{1}{2}}^n - \mathcal{F}_{k+1,j-\frac{1}{2}}^n}{\Delta x} + \frac{v_0}{2} \frac{\mathcal{F}_{k-1,j+\frac{1}{2}}^n - \mathcal{F}_{k-1,j-\frac{1}{2}}^n}{\Delta x} = 0, \quad (5.3)$$

in which the numerical ‘kinetic-based’ fluxes are evaluated based on the approximation  $f_N$  [10, 19]. For instance, we have

$$\mathcal{F}_{k,j+\frac{1}{2}} = \int_{(-\frac{\pi}{2}, \frac{\pi}{2})} e^{ik\theta} f_j(\theta) d\theta + \int_{(-\pi, -\frac{\pi}{2}) \cup (\frac{\pi}{2}, \pi)} e^{ik\theta} f_{j+1}(\theta) d\theta.$$

Substituting the ansatz Eq.(2.5) or (3.9) for  $f(\theta)$  to the above integrands, we see that only the integrals of the form  $\int e^{ik\theta} P_r(\phi - \theta) d\theta$  and  $\ell \int e^{ik\theta} d\theta$  need to be computed. For the latter type, it is easy to derive

$$\ell \int_{-\frac{\pi}{2}}^{\frac{\pi}{2}} e^{ik\theta} d\theta = \frac{\ell}{ik} (e^{ik\frac{\pi}{2}} - e^{-ik\frac{\pi}{2}}) = \frac{2\ell}{k} \sin\left(\frac{k\pi}{2}\right).$$

In what follows we deduce an analytical expression for

$$I_k := \int_{-\frac{\pi}{2}}^{\frac{\pi}{2}} e^{ik\theta} P_r(\phi - \theta) d\theta,$$

whereas the integration on other types of intervals can be handled similarly.

With the Fourier series of the Poisson kernel  $P_r(\phi - \theta) = \frac{1}{2\pi} \sum_{m \in \mathbb{Z}} r^{|m|} e^{-im(\phi - \theta)}$ , we obtain

$$\begin{aligned} I_k &= \frac{1}{2\pi} \sum_{m \in \mathbb{Z}} r^{|m|} e^{-im\phi} \int_{-\frac{\pi}{2}}^{\frac{\pi}{2}} e^{i(k+m)\theta} d\theta \\ &= \frac{r^{|k|} e^{ik\phi}}{2} + \frac{1}{2\pi} \sum_{m \neq -k} \frac{r^{|m|} e^{-im\phi} (e^{i(k+m)\frac{\pi}{2}} - e^{-i(k+m)\frac{\pi}{2}})}{i(k+m)} \\ &= \frac{r^{|k|} e^{ik\phi}}{2} + \frac{e^{ik\phi}}{2\pi i} \sum_{m \neq 0} \frac{r^{|m-k|} e^{-im\phi} (e^{im\frac{\pi}{2}} - e^{-im\frac{\pi}{2}})}{m}. \end{aligned}$$

With  $k > 0$ , it is clear that we need to compute summations of the form

$$\begin{aligned} \sum_{m \neq 0} \frac{r^{|m-k|} z^m}{m} &= \sum_{m < 0} \frac{r^{k-m} z^m}{m} + \sum_{m=1}^k \frac{r^{k-m} z^m}{m} + \sum_{m \geq k+1} \frac{r^{m-k} z^m}{m} \\ &= \sum_{m < 0} \frac{r^{k-m} z^m}{m} + \sum_{m=1}^k \frac{(r^{k-m} - r^{m-k}) z^m}{m} + \sum_{m \geq 1} \frac{r^{m-k} z^m}{m} \\ &= r^k \ln(1 - rz^{-1}) + \sum_{m=1}^k \frac{(r^{k-m} - r^{m-k}) z^m}{m} - r^{-k} \ln(1 - rz). \end{aligned}$$

The last equality follows from the formal series for  $|z| < 1$ :

$$G(z) = \sum_{m \geq 1} \frac{z^m}{m} = -\ln(1 - z).$$

To see this, just notice  $G'(z) = \sum_{m \geq 0} z^m = (1 - z)^{-1}$ .

As a consequence, we further proceed  $I_k$  as

$$\begin{aligned} &\sum_{m \neq 0} \frac{r^{|m-k|} e^{-im\phi} (e^{im\frac{\pi}{2}} - e^{-im\frac{\pi}{2}})}{m} \\ &= -r^k \ln \frac{1 - ire^{i\phi}}{1 + ire^{i\phi}} + r^{-k} \ln \frac{1 + ire^{-i\phi}}{1 - ire^{-i\phi}} + \sum_{m=1}^k (i^m - (-i)^m) \frac{r^{k-m} - r^{m-k}}{m} e^{-im\phi}. \end{aligned}$$

If  $k < 0$  (note that  $m_{-1}$  is involved in the system),  $I_k$  can be computed by the same technique, with the results presented below.

$$\begin{aligned} &\sum_{m \neq 0} \frac{r^{|m-k|} e^{-im\phi} (e^{im\frac{\pi}{2}} - e^{-im\frac{\pi}{2}})}{m} \\ &= -r^k \ln \frac{1 - ire^{i\phi}}{1 + ire^{i\phi}} + r^{-k} \ln \frac{1 + ire^{-i\phi}}{1 - ire^{-i\phi}} + \sum_{m=1}^{-k} (i^m - (-i)^m) \frac{r^{-k-m} - r^{m+k}}{m} e^{im\phi}. \end{aligned}$$

**5.2. Collision term.** Eq.(5.2) is treated with a first-order semi-implicit scheme, which reads as

$$\frac{\epsilon}{\Delta t} (m_k^{n+1} - m_k^*) = -\mathbf{d}k^2 m_k^{n+1} + \mathbf{1}_{|m_1^*| > 0} \cdot \frac{\nu k}{2|m_1^*|} (m_1^* m_{k-1}^{n+1} - \overline{m_1^*} m_{k+1}^{n+1})$$

for  $k = 0, 1, \dots, N-1$ , and

$$\frac{\epsilon}{\Delta t} (m_N^{n+1} - m_N^*) = -\mathbf{d}N^2 m_N^{n+1} + \mathbf{1}_{|m_1^*| > 0} \cdot \frac{\nu N}{2|m_1^*|} (m_1^* m_{N-1}^{n+1} - \overline{m_1^*} \hat{m}_{N+1}^n)$$

for the last moment  $m_N$ . The above equations are concisely collected as

$$\begin{bmatrix} \gamma & 0 & & & \\ \ddots & \ddots & \ddots & & \\ & -\alpha k & \gamma + dk^2 & \bar{\alpha}k & \\ & & \ddots & \ddots & \ddots \\ & & & -\alpha N & \gamma + dN^2 \end{bmatrix} \begin{bmatrix} m_0^{n+1} \\ \vdots \\ m_k^{n+1} \\ \vdots \\ m_N^{n+1} \end{bmatrix} = \gamma \begin{bmatrix} m_0^* \\ \vdots \\ m_k^* \\ \vdots \\ m_N^* \end{bmatrix} + \begin{bmatrix} 0 \\ \vdots \\ 0 \\ \vdots \\ -\bar{\alpha}N\hat{m}_{N+1}^n \end{bmatrix}$$

with  $\alpha = \frac{\nu m_1^*}{2|m_1^*|}$  and  $\gamma = \frac{\epsilon}{\Delta t}$ .

During the simulation, the time step  $\Delta t$  is chosen to satisfy the CFL condition while ensuring that the above coefficient matrix is strictly diagonally dominant:

$$\Delta t < \frac{\epsilon}{\nu k - dk^2}.$$

**5.3. Boundary conditions.** Three kinds of boundary conditions are used in this work, including the Neumann condition, the periodic boundary and the reflexive wall boundary. For the last one, it is assumed that all particles rebound elastically with no flux into the wall. Let  $x_b$  be the 1-D wall position and  $x > x_b$  the physical domain. Then at the kinetic level, the reflexive condition reads as

$$f(x_b, \theta) = f(x_b, \pi - \theta) \quad \text{for} \quad -\frac{\pi}{2} \leq \theta \leq \frac{\pi}{2}.$$

In this way, the kinetic-based flux can be evaluated as

$$\int_{-\frac{\pi}{2}}^{\frac{\pi}{2}} f(\theta) e^{ik\theta} d\theta = - \int_{\frac{\pi}{2}}^{\frac{3\pi}{2}} f(\theta) e^{ik(\pi-\theta)} d\theta = -e^{ik\pi} \overline{\int_{\frac{\pi}{2}}^{\frac{3\pi}{2}} f(\theta) e^{-ik\theta} d\theta}.$$

## 6. NUMERICAL RESULTS

This section is devoted to a series of numerical tests including spatially homogeneous, 1D and 2D cases. Comparison with the analytical solution, the macroscopic limit and the microscopic particle simulation is provided to show the validity of our Poisson-EQMOM. In the subsequent subsections, we set  $\nu = 1$  and  $d = 0.2$  in Eq.(4.1) for all cases. Overall, it is demonstrated that the Poisson-EQMOM produces reasonable results in all cases.

**6.1. Spatially homogeneous case.** Inspired by [13], we first validate our computational model by a spatially homogeneous case  $\partial_t f = Q(f)$  to test the convergence of the numerical results towards the known equilibrium of  $Q(f)$ , a von Mises distribution in Eq.(4.3). For such case, the initial distribution is specified as

$$f_0(\theta) = (1 + \cos(4\theta)) \cdot \exp \left( -\cos \left( \pi \left( \frac{\theta}{2\pi} + \left( \frac{\theta}{2\pi} \right)^4 \right) \right) \right)$$

for  $\theta \in [-\pi, \pi)$  with its moments  $m_k(t=0)$  approximated by

$$m_k(0) = \sum_{j=0}^{1023} f_0(-\pi + j\Delta\theta) e^{ikj\Delta\theta} \Delta\theta, \quad \Delta\theta = \frac{2\pi}{1024}.$$

Using the schemes in subsection 5.2 and a CFL number of 0.5, we simulate the time evolution of  $f(\theta)$  with the 8-node Poisson-EQMOM. It is worth mentioning that the use of moment methods preserves mass conservation naturally. As plotted in Fig. 3a, after a sufficiently long duration time ( $t = 20$ ), the reconstructed distribution  $f$  is in good agreement with the von Mises distribution peaked at  $\bar{\theta} = -0.6523\pi$ . Fig. 3b quantifies the time-evolved  $L^2$ -errors  $\|f(\theta) - M_{\bar{\theta}}(\theta)\|_{L^2}$  between the reconstructed distribution and the equilibrium at that time. We see exponential convergence at the initial stage. Moreover, with an increase of  $N$  from 4 to 32, the error reduces substantially.

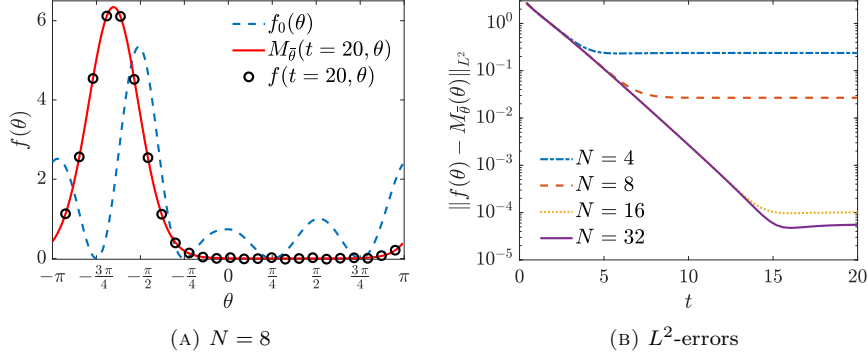


FIGURE 3. The spatially homogeneous case.

**6.2. 1D Riemann problems.** Our second case is the spatially one-dimensional Riemann problems with the initial conditions characterized by the density  $\rho = m_0$  and the macroscopic velocity direction  $\bar{\theta} = \arg m_1$ . As demonstrated in [13], the 1D problems provide ideal situations to test the performance of numerical methods in the hydrodynamic regime where the scaling factor  $\epsilon$  in Eq.(4.1) approaches zero. In such a scenario, both the density and velocity direction obtained with the kinetic equation are expected to converge, as  $\epsilon \rightarrow 0$ , to those solved from the hydrodynamic model.

In the simulation, the computational domain  $x \in [-5, 5]$  is divided into 1000 uniform grids. For the initial conditions, we set  $(\rho_l, \bar{\theta}_l)$  for  $x < 0$  and  $(\rho_r, \bar{\theta}_r)$  for  $x > 0$ . Then the initial moments  $m_k(0, x)$  are computed with the von Mises distribution determined by the macroscopic quantities. In all problems, we choose  $N = 12$  for the Poisson-EQMOM and the CFL number of 0.5. The Neumann boundary condition is employed at both ends  $x = \pm 5$ .

Our initial data follow [13]. The first case is given by

$$(\rho_l, \bar{\theta}_l) = (2, 1.7), \quad (\rho_r, \bar{\theta}_r) = (0.218, 0.5), \quad (6.1)$$

in which a rarefaction wave forms in the hydrodynamic model. The second case generates a shock wave and the initial conditions read as

$$(\rho_l, \bar{\theta}_l) = (1, 1.5), \quad (\rho_r, \bar{\theta}_r) = (2, 1.83). \quad (6.2)$$

The third one is a contact discontinuity:

$$(\rho_l, \bar{\theta}_l) = (1, 1), \quad (\rho_r, \bar{\theta}_r) = (1, -1). \quad (6.3)$$

The simulated profiles of  $\rho$  and  $\bar{\theta}$  at  $t = 4$  are presented in Figs. 4-6 for three values of  $\epsilon$ . Also shown in each plot is the solution of the hydrodynamic model extracted from [13]. It is clearly seen that with  $\epsilon$  approaching 0, the Poisson-EQMOM predicted  $\rho$  and  $\bar{\theta}$  become quite close to the macroscopic solutions in all cases, well capturing the drastic change across the wave fronts. This serves as convincing evidence of the reliability of our computational model.

**6.3. Spatially 2D cases.** In this subsection, several spatially 2D simulations are performed on a physical domain  $(x, y) \in [-5, 5] \times [-5, 5]$  employing different boundary conditions. The domain is divided into  $50 \times 50$  uniform grids, resulting in  $\Delta x = \Delta y = 0.2$ . We set  $\epsilon = 1$  in Eq.(4.1) for comparisons with the microscopic simulation results. Throughout this subsection we choose  $N = 4$  for the Poisson-EQMOM and the CFL number of 0.25.

The initial condition is generated with a constant density  $m_{0,ij}(t = 0) = 1$ , and the higher-order moments are determined by the von Mises distributions with the mean velocity direction  $\bar{\theta}_{ij}$  uniformly distributed on  $[-\pi, \pi]$  for all  $1 \leq i, j \leq 50$ . Our simulation marches in time to examine specific long-time patterns.



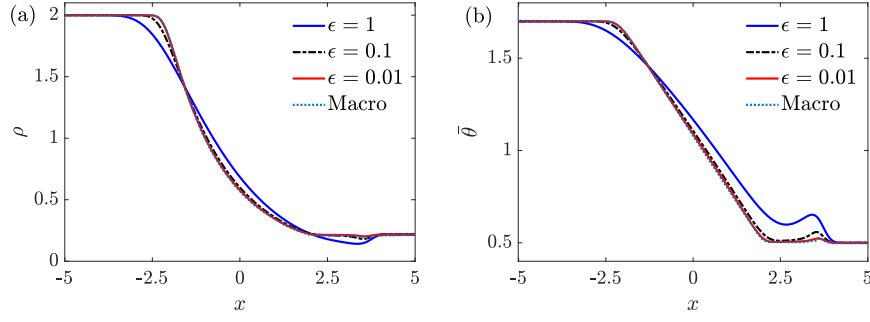


FIGURE 4. The 1D Riemann problem (6.1) with a rarefaction wave. The profiles of density  $\rho$  and velocity direction  $\bar{\theta}$  at  $t = 4$ . The ‘macro’ profiles are extracted from [13].

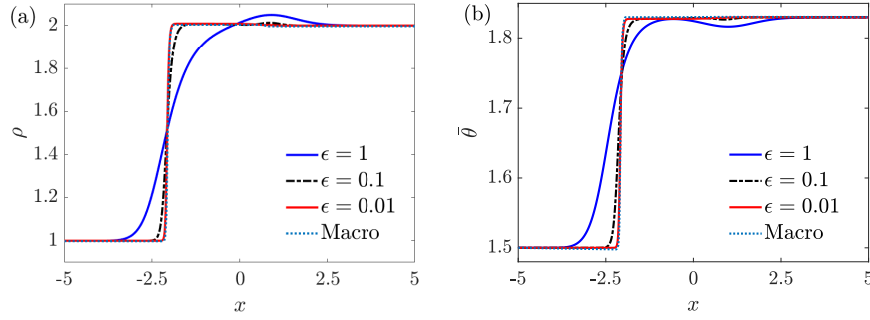


FIGURE 5. The 1D Riemann problem (6.2) with a shock wave. The profiles of density  $\rho$  and velocity direction  $\bar{\theta}$  at  $t = 4$ . The ‘macro’ profiles are extracted from [13].

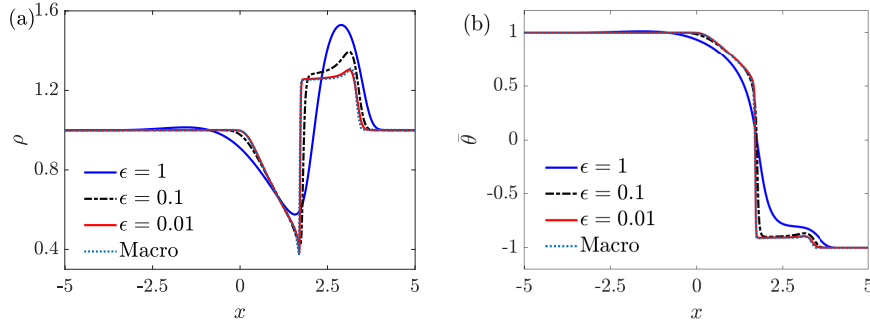


FIGURE 6. The 1D Riemann problem (6.3) with a contact discontinuity. The profiles of density  $\rho$  and velocity direction  $\bar{\theta}$  at  $t = 4$ . The ‘macro’ profiles are extracted from [13].

For a comparison, the microscopic Vicsek model is simulated on the same domain using 10 000 particles. A continuous version of the Vicsek model is applied here [9, 13]. The particle speed is 1. The radius of interaction is 0.2 and the discrete time step is taken as 0.01. The intensity of noise  $d = 0.2$ . Similarly, at the initial state, the particles are uniformly distributed in space and velocity direction. If the wall condition is present, each impacting particle reflects with its normal velocity component reversed.

**6.3.1. Periodic boundaries.** We first consider the case with four periodic boundary conditions. In this case, for any function  $\phi = \phi(t, x, y)$ , we have

$$\phi(t, x, y) = \phi(t, x + 10p, y + 10q)$$

for any  $p, q \in \mathbb{Z}$ . Fig. 7 shows the typical density and velocity distributions at  $t = 200$  predicted by both the 4-node Poisson-EQMOM and the particle model. It is clearly seen that, under such a noise strength ( $d = 0.2$ ), the long-time behavior is a global alignment state with nearly homogeneous density in space, even though the coarse-grained result from the particle model exhibits larger extent of fluctuations. Thus, our Poisson-EQMOM produces reasonable results at the kinetic level, which is consistent with the particle model in this case.

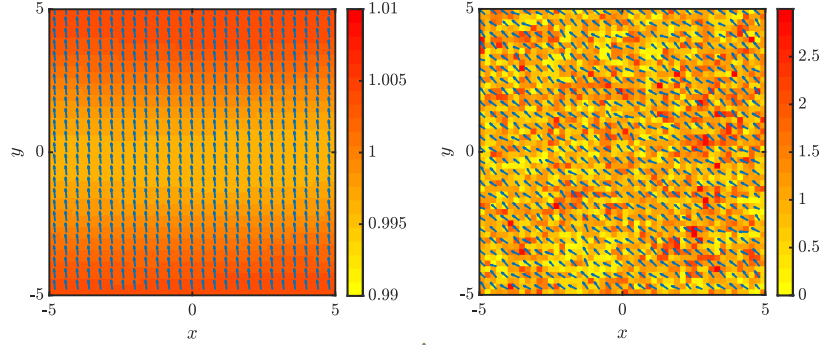


FIGURE 7. Density and velocity distributions at  $t = 200$  by the 4-node Poisson-EQMOM (Left) and the Vicsek model (Right) for the 2D case with periodic boundary conditions.

**6.3.2. Two reflexive walls.** Our second case sets the boundaries  $x = \pm 5$  as reflexive walls, leaving  $y = \pm 5$  still as periodic conditions. That is,  $\phi(t, x, y) = \phi(t, x, y + 10q)$  for any function  $\phi$  and  $q \in \mathbb{Z}$ . The time evolution of the density and velocity distributions is plotted in Fig. 8 for different snapshots, showing a more complex pattern than those of the previous case with all periodic conditions. After a transient period, the system is observed to have converged to a density-oscillating state between the opposite walls with a full cycle lasting about 40 unit time, as revealed at both the kinetic (Figs. 8a,c,e) and microscopic (Figs. 8b,d,f) levels. The snapshots in Fig. 8 cover half of the cycle: the bulk density is moving to the left, generating a huge peak adjacent to the left wall in Figs. 8c&d, and then goes back towards the right wall. The consistency of the micro- and meso-scales again justifies our use of the Poisson-EQMOM.

It is interesting to point out some features of the system. In the near-wall region, the particles move almost along the wall because the normal velocity components are eliminated due to particle rebound and the alignment interaction. By contrast, particles migrate along the  $x$ -axis far away from the wall, transporting the ‘density wave front’ back and forth at a mean ‘bulk’ velocity about 0.5. The crowded area can be 5-7 times denser than the most sparse region. However, it is postulated that this density inhomogeneity may be distinct from the ‘phase separation’ state [8] which is believed to exist at larger noise strengths. The kinetic simulation implies that the low-density regions here

are still aligned effectively and are thus not suitable to be regarded as a disordered state (with zero macroscopic speed). A thorough investigation is beyond our current scope and will be left for future work.

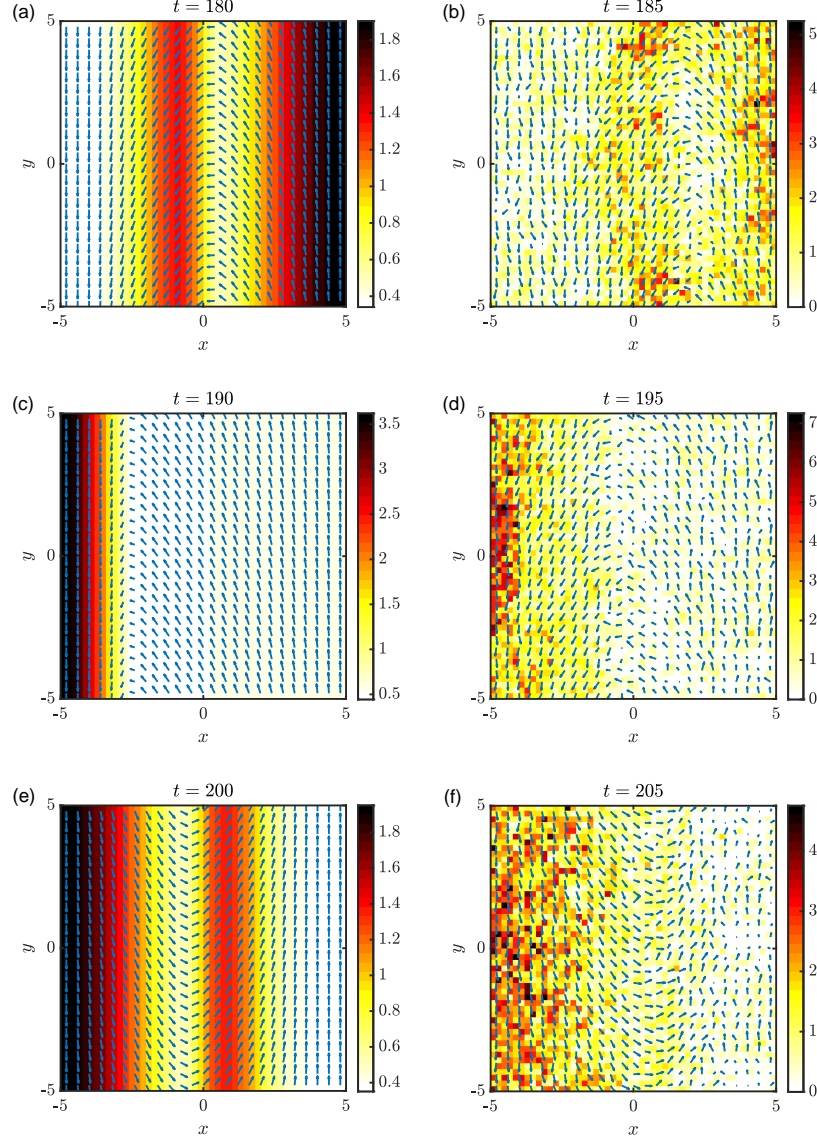


FIGURE 8. Density and velocity distributions at different snapshots for the 2D case with two reflexive walls located at  $x = \pm 5$ . Periodic conditions are imposed on  $y = \pm 5$ . Left column: 4-node Poisson-EQMOM; Right column: Vicsek model. The snapshots cover half of the full density-oscillating cycle.

**6.3.3. Four walls with vortex formation.** Having witnessed the intriguing pattern induced by walls, we further assume in this case that the domain is entirely bounded by reflexive walls. As shown in Fig. 9, after a transient period, both the kinetic and particle simulations predict a stable bulk vortex rotating around the origin with the particle density concentrating adjacent to the walls. As a result, the center is nearly empty. The same pattern was reported in [13]. The vortex forms because each wall

drives the particles to stream along, so the period of rotation is around 40 unit time. On the other hand, there is a lack of mechanism that effectively transports particles away from the wall, leading to mass accumulation near the wall and a central void, which in turn strengthen the alignment in the ‘tangential’ direction. We can tell from the velocity field that the particles are locally aligned while having a global flow structure.

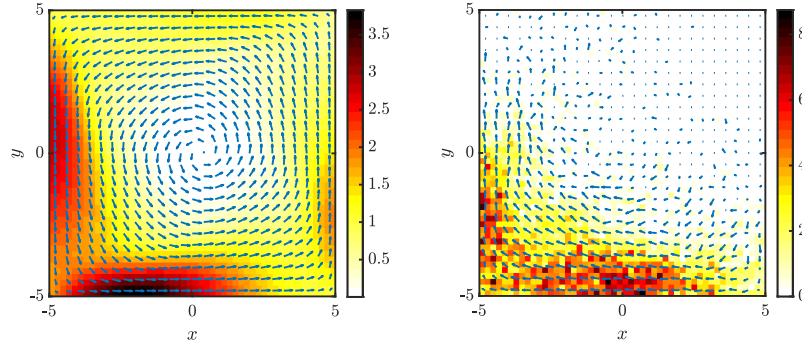


FIGURE 9. Density and velocity distributions at  $t = 200$  for the 2D case with four reflexive walls: (Left) 4-node Poisson-EQMOM; (Right) Vicsek model.

## 7. CONCLUSIONS

This paper develops a novel moment method, called the Poisson-EQMOM, for 2D kinetic equations with velocity of constant magnitude. The idea is to approximate the distribution function with a convex combination of finite shifted homoscedastic Poisson kernels. The application of the Poisson-EQMOM to a KE-VC associated with the seminal Vicsek model generates a reliable moment closure system.

Besides being *positivity-preserving* and *of the conservative form*, the Poisson-EQMOM is shown to be well defined for *all* physically relevant moments. More importantly, as long as the original distribution has a positive lower bound, the resultant approximation *converges* as the number of moments goes to infinity. The proofs are quite technical and crucially rely on the choice of Poisson kernel. Based on these nice properties, we devise a robust moment inversion algorithm. This algorithm involves a ‘lifting’ technique to efficiently enhance the approximation precision while reducing the computational complexity. The centers of the Poisson modes are computed with the aid of the orthogonal polynomial theory on the unit circle.

The Poisson-EQMOM is numerically validated with the moment system based on the Vicsek model, where a delicate treatment of the kinetic-based flux is involved. For all test cases ranging from spatially homogeneous to 2D, the numerical results are satisfactory. Precisely, the results converge in time to the analytical homogeneous solutions, well capture the flow discontinuities at the macroscopic level, and reveal fascinating wall-induced patterns in consistent with the microscopic simulations. The success in the Vicsek dynamics indicates a potential of using the Poisson-EQMOM to study more types of model and the wall influences on the active flow structure.

## ACKNOWLEDGMENTS

The authors owe their sincere appreciation to Prof. Hui Yu at Tsinghua University for her kind assistance in particle simulations of the Vicsek model. The authors are also grateful to Prof. Pierre Degond at CNRS, Prof. Shuiqing Li and Mr. Hanlin Lin at Tsinghua University, and Prof. Xianmin Xu at CAS for the insightful discussions.

## APPENDIX A.

*Proof of Theorem 2.2.* For both  $f$  and  $f_N$ , recall the Fourier series

$$f = \frac{1}{2\pi} \sum_{k \in \mathbb{Z}} \hat{f}(k) e^{ik\theta}, \quad f_N = \frac{1}{2\pi} \sum_{k \in \mathbb{Z}} \hat{f}_N(k) e^{ik\theta}$$

with  $\hat{f}(k) = \overline{m_k}$  for all  $k \in \mathbb{Z}$  and  $\hat{f}_N(k) = \hat{f}(k)$  for  $|k| = 0, \dots, N$ . On the other hand, we see from Eqs.(2.5 & 2.7) that

$$\begin{aligned} f_N &= \left( \sum_{|k| \leq N} + \sum_{|k| > N} \right) \frac{r_N^{|k|}}{2\pi} \left( \sum_{\alpha=1}^N \rho_{\alpha,N} e^{ik\phi_{\alpha,N}} \right) e^{-ik\theta} \\ &= \sum_{|k| \leq N} \hat{f}(k) e^{ik\theta} + \sum_{|k| > N} e^{ik\theta} r_N^{|k|} \cdot O(1), \end{aligned}$$

in which the  $N$ -dependence of  $\rho_\alpha$ ,  $\phi_\alpha$  and  $r$  is explicitly presented. The second term of the last expression contains  $O(1)$  because  $|\sum \rho_\alpha e^{ik\phi_\alpha}| \leq \sum \rho_\alpha = m_0$ .

Then we have, for any  $2 \leq p < \infty$ , that

$$\begin{aligned} \|f_N - f\|_{L^p} &\leq \|f_N - \sum_{|k| \leq N} \hat{f}(k) e^{ik\theta}\|_{L^p} + \left\| \sum_{|k| > N} \hat{f}(k) e^{ik\theta} \right\|_{L^p} \\ &\leq C \left( \sum_{|k| > N} r_N^{kp'} \right)^{\frac{1}{p'}} + \left\| \sum_{|k| > N} \hat{f}(k) e^{ik\theta} \right\|_{L^p} \end{aligned} \quad (\text{A.1})$$

with  $p' = 1/(1-p^{-1}) \in (1, 2]$ . The last step follows from the Hausdorff-Young's inequality. Hereinafter  $C$  denotes a finite positive constant.

We also need the fact that  $\lim_{N \rightarrow \infty} r_N$  exists because the sequence  $\{r_N\} \subset [0, 1]$  is increasing. To see this, notice that the minimum eigenvalue of  $H_{N-1}(\mathbf{M}_N^*(r_{N-1}))$  is zero, implying  $\lambda(r_{N-1}; N) \leq 0$ . Since  $\lambda(r_N; N) = 0$  and  $\lambda(r; N)$  is strictly increasing on  $r$  (Proposition 2.2), it is only possible that  $r_N \geq r_{N-1}$ .

(i). Using  $f' \in L^2(-\pi, \pi)$ , we obtain from the Parseval's theorem that

$$\infty > \int |f'|^2 d\theta = \sum_{k \in \mathbb{Z}} |\hat{f}'(k)|^2 = \sum_{k \in \mathbb{Z}} k^2 |m_k|^2.$$

As a consequence, the series  $\sum_{|k| \leq N} \overline{m_k} e^{ik\theta} \rightarrow 2\pi f$  uniformly as  $N \rightarrow \infty$  because

$$\left| \sum_k \overline{m_k} e^{ik\theta} \right|^2 \leq \left( \sum_k |k \overline{m_k} e^{ik\theta}|^2 \right) \left( \sum_k k^{-2} \right) < \infty.$$

This fact immediately leads to  $\left\| \sum_{|k| > N} \hat{f}(k) e^{ik\theta} \right\|_{L^2} \rightarrow 0$  as  $N \rightarrow \infty$ . Thanks to Eq.(A.1), it then suffices to show

$$\sum_{k > N} r_N^{2k} = \frac{r_N^{2N+2}}{1 - r_N^2} \leq C \frac{r_N^{2N}}{1 - r_N} \rightarrow 0 \quad \text{as } N \rightarrow \infty, \quad (\text{A.2})$$

which holds trivially if  $\lim r_N < 1$ . As such, in what follows we shall assume  $\lim r_N = 1$ .

As we need only to consider very large  $N$ , one can specify a sufficiently large  $n \leq N$  such that

$$\sum_{|k| < n} \overline{m_k} e^{ik\theta} \geq c\pi \quad \text{and} \quad \sum_{|k| \geq n} k^2 |m_k|^2 < \delta_n \rightarrow 0^+, \quad (\text{A.3})$$

which are both consequences of  $f' \in L^2$ .

Take  $a = (a_0, \dots, a_N) \in \mathbb{C}^{N+1}$  and define

$$\begin{aligned} q_N(r; a) &:= \bar{a}^T H_N(\mathbf{M}_N^*(r)) a = \sum_{k,l=0}^N \bar{a}_k a_l m_{l-k} r^{-|l-k|} \\ &= \frac{1}{2\pi} \int_{-\pi}^{\pi} |a(\theta)|^2 \left( \sum_{|k| \leq N} r^{-|k|} \overline{m_k} e^{ik\theta} \right) d\theta \end{aligned} \quad (\text{A.4})$$

with  $a(\theta) = \sum_l a_l e^{il\theta}$ . The last expression can be verified by applying the orthogonality of the bases  $e^{ik\theta}$ . Since  $H_N(\mathbf{M}_N^*(r_N))$  is singular, there exists  $\tilde{a} \in \mathbb{C}^{N+1}$  with  $\|\tilde{a}\| = 1$  such that

$$0 = |q_N(r_N; \tilde{a})| = |A + B| \geq |A| - |B|.$$

Here we denote

$$A = \frac{1}{2\pi} \int_{-\pi}^{\pi} |\tilde{a}(\theta)|^2 \left( \sum_{|k| < n} r_N^{-|k|} \overline{m_k} e^{ik\theta} \right) d\theta.$$

Recall  $\lim r_N = 1$ . Take a sufficiently large  $N$  with  $r_N$  so close to 1 that the real finite sum  $\sum_{|k| < n} r_N^{-|k|} \overline{m_k} e^{ik\theta}$  is close to  $\sum_{|k| < n} \overline{m_k} e^{ik\theta}$ . Considering Eq.(A.3), one may require  $\sum_{|k| < n} r_N^{-|k|} \overline{m_k} e^{ik\theta} \geq c\pi/2$  and hence  $A \geq c\pi/2$  (because  $\int |\tilde{a}(\theta)|^2 d\theta = 2\pi$ ).

For the rest part  $B = q_N(r_N; \tilde{a}) - A$ , we have

$$\begin{aligned} |B|^2 &\leq \left( \sum_{|k|=n}^N r_N^{-|k|} |m_k| \right)^2 \leq 4 \left( \sum_{k=n}^N k^{-2} r_N^{-2k} \right) \left( \sum_{k=n}^N k^2 |m_k|^2 \right) \\ &\leq 8\delta_n \sum_{k=n}^N \frac{r_N^{-2k}}{k(k+1)} \leq 8\delta_n \left( \frac{r_N^{-2n}}{n} + (1 - r_N^2) r_N^{-2N} \sum_{k=n+1}^N \frac{r_N^{2N-2k}}{k} \right). \end{aligned} \quad (\text{A.5})$$

Using  $1 + r_N \leq 2$  and  $\sum_{k=n+1}^N k^{-1} r_N^{2N-2k} \leq \sum_{k=n+1}^N k^{-1} \leq 2 \log N$ , we deduce from the inequality  $|A| \leq |B|$  that

$$\delta_n \left( C(1 - r_N) r_N^{-2N} \log N + O\left(\frac{1}{n}\right) \right) \geq \left( \frac{c\pi}{2} \right)^2 > 0.$$

With both  $N \geq n \rightarrow \infty$ , it is seen that  $\delta_n \rightarrow 0^+$  and hence

$$(1 - r_N) r_N^{-2N} \log N \rightarrow \infty \quad \text{as } N \rightarrow \infty. \quad (\text{A.6})$$

We then claim that the sequence  $\{r_N^N \log N\}$  is uniformly bounded. Otherwise there exists an unbounded subsequence  $\{r_T^T \log T\}$  (indexed with  $T$ ) which must satisfy  $r_T^T \geq (\log T)^{-1}$  for large  $T$ . On the other hand, Eq.(A.6) implies that for large  $T$ , we have  $1 - r_T \geq r_T^{2T} (\log T)^{-1} \geq (\log T)^{-3}$ . This leads to

$$\begin{aligned} \log(r_T^T \log T) &\leq T \log(1 - (\log T)^{-3}) + \log \log T \\ &\leq -T(\log T)^{-3} + \log \log T \rightarrow -\infty \quad \text{as } T \rightarrow \infty, \end{aligned}$$

a contradiction to the unboundedness of  $\{r_T^T \log T\}$ .

Now the estimation in Eq.(A.5) can be refined by computing

$$\sum_{k=1}^N \frac{r_N^{2N-2k}}{k} = \left( \sum_{k=1}^{\lfloor \frac{N}{2} \rfloor} + \sum_{k=\lfloor \frac{N}{2} \rfloor + 1}^N \right) \frac{r_N^{2N-2k}}{k} \leq 2(r_N^N \log N + \log 2) < \infty.$$

As a result, the inequality  $|A| \leq |B|$  gives

$$\delta_n \left( C(1 - r_N) r_N^{-2N} + O\left(\frac{1}{n}\right) \right) \geq \left( \frac{c\pi}{2} \right)^2 > 0.$$

By letting  $N \geq n \rightarrow \infty$ , we thus derive the desired estimate for  $r_N$  in Eq.(A.2).

(ii). If  $f$  is Lipschitz,  $f'$  is uniformly bounded and  $f' \in L^2(-\pi, \pi)$ . According to Eq.(A.1), it suffices to show, for  $p' \in (1, 2]$ ,

$$\sum_{k \geq N} r_N^{kp'} = \frac{r_N^{p'(N+1)}}{1 - r_N^{p'}} \leq C \frac{r_N^{Np'}}{1 - r_N} \rightarrow 0 \quad \text{as } N \rightarrow \infty. \quad (\text{A.7})$$

Similarly, we only need to deal with the case  $\lim r_N = 1$ .

Our strategy is to establish an estimation related to the lower and upper bounds of the integration  $\int |\partial_r q_N(r; a)| dr$ . Here  $q_N(r; a)$  is defined in Eq.(A.4) for  $a \in \mathbb{C}^{N+1}$  and  $\|a\| = 1$ . We compute

$$q_N(1; a) = \frac{1}{2\pi} \int_{-\pi}^{\pi} |a(\theta)|^2 \left( \sum_{|k| \geq N} \overline{m_k} e^{ik\theta} \right) d\theta = \frac{1}{2\pi} \int_{-\pi}^{\pi} |a(\theta)|^2 f(\theta) d\theta \geq c,$$

where the second equality follows from the orthogonality of the bases  $e^{ik\theta}$ . Specify  $a$  such that  $q_N(r_N; a) = 0$ , and then we have

$$\int_{r_N}^1 |\partial_r q_N(r; a)| dr \geq |q_N(1; a) - q_N(r_N; a)| \geq c. \quad (\text{A.8})$$

The upper bound needs the detailed form of the derivative

$$\partial_r q_N(r; a) = -\frac{r^{-1}}{2\pi} \int_{-\pi}^{\pi} |a(\theta)|^2 g(\theta) d\theta$$

with

$$\begin{aligned} g(\theta) &= \sum_{|k| \leq N} |k| r^{-|k|} \overline{m_k} e^{ik\theta} = 2 \sum_{k=1}^N k r^{-k} \Re(m_{-k} e^{ik\theta}) \\ &= 2 \sum_{k=1}^N k r^{-k} \int_{-\pi}^{\pi} f(t + \theta) \cos kt dt = -2 \int_{-\pi}^{\pi} f'(t + \theta) \left( \sum_{k=1}^N r^{-k} \sin kt \right) dt. \end{aligned}$$

To derive an upper bound, we compute

$$\begin{aligned} \sum_{k=1}^N r^{-k} \sin kt &= \Im \sum_{k=1}^N (r^{-1} e^{it})^k = \Im \frac{1 - r^{-N} e^{iNt}}{r e^{-it} - 1} \\ &= \frac{(1 - r) r^{-N} \sin Nt + r^{1-N} (\sin Nt - \sin(N+1)t) + r \sin t}{1 - 2r \cos t + r^2} \end{aligned}$$

and try to control each term. Here  $\Im(z)$  denotes the imaginary part of  $z \in \mathbb{C}$ . Suppose  $r > \frac{1}{2}$ , which can be satisfied for large  $N$ . With the property  $\sin(t/2) \geq t/\pi$  for  $|t| \leq \pi$ , it holds true that

$$\frac{|\sin t|}{1 - 2r \cos t + r^2} = \frac{|\sin t|}{(1 - r)^2 + 4r \sin^2(\frac{t}{2})} \leq \frac{|t|}{(1 - r)^2 + 2(\frac{t}{\pi})^2} \leq \frac{C|t|}{(1 - r)^2 + t^2},$$

resulting in

$$\int_{-\pi}^{\pi} \frac{|\sin t|}{1 - 2r \cos t + r^2} dt \leq C \int_0^{\pi} \frac{2t}{(1 - r)^2 + t^2} dt = C \log \left[ 1 + \left( \frac{\pi}{1 - r} \right)^2 \right].$$

Noticing  $|\sin Nt - \sin(N+1)t| = 2|\sin \frac{t}{2} \cos(N + \frac{1}{2})t| \leq 2|\sin \frac{t}{2}|$ , we obtain

$$\begin{aligned} |\partial_r q_N(r; a)| &\leq \|r^{-1} g\|_{L^\infty} \leq C \int_{-\pi}^{\pi} \left| r^{-1} \sum_{k=1}^N r^{-k} \sin kt \right| dt \\ &\leq C r^{-N} + C(r^{-N} + 1) \log \left[ 1 + \left( \frac{\pi}{1 - r} \right)^2 \right] \end{aligned}$$

for  $r$  sufficiently close to 1. To evaluate the integration, a technical result is needed:

$$\begin{aligned} \int_{r_N}^1 \log \left[ 1 + \left( \frac{\pi}{1-r} \right)^2 \right] dr &= \int_0^{1-r_N} \log \left( 1 + \frac{\pi^2}{t^2} \right) dt \\ &= (1-r_N) \log \left( 1 + \frac{\pi^2}{(1-r_N)^2} \right) + \int_0^{1-r_N} \frac{2\pi^2}{t^2 + \pi^2} dt \\ &\leq (1-r_N) \left[ \log \left( 1 + \frac{\pi^2}{(1-r_N)^2} \right) + 2 \right], \end{aligned}$$

where the integration by parts has been used. Therefore, by applying  $1 \leq r^{-N} \leq r_N^{-N}$  for  $r_N \leq r \leq 1$ , we get

$$\begin{aligned} c &\leq \int_{r_N}^1 |\partial_r q_N(r; a)| dr \leq C r_N^{-N} \int_{r_N}^1 \log \left[ 1 + \left( \frac{\pi}{1-r} \right)^2 \right] dr \\ &\leq C r_N^{-N} (1-r_N) \log \left[ 1 + \left( \frac{\pi}{1-r_N} \right)^2 \right] \\ &\leq C r_N^{-N} (1-r_N)^{\frac{1}{p'} + \epsilon} \end{aligned} \tag{A.9}$$

for any  $0 < \epsilon < 1 - \frac{1}{p'}$  because  $\lim_{x \rightarrow 0^+} x^\delta \log x = 0$  for any  $\delta > 0$ . Rearranging the above inequality as  $r_N^{Np'} (1-r_N)^{-1} \leq C (1-r_N)^{\epsilon p'}$  gives Eq.(A.7) immediately.

(iii). Suppose for the sake of contradiction that  $f_N$  does not converge to  $f$  uniformly. Then there exists a subsequence  $\{r_T\}$  (indexed with  $T$ ) satisfying

$$r_T^{-T} (1-r_T) \leq C.$$

Otherwise we have  $r_N^N / (1-r_N) \rightarrow 0$  as  $N \rightarrow \infty$ , which implies uniform convergence because  $|f_N - f| = \left| \sum_{|k| > N} e^{ik\theta} r_N^{|k|} O(1) \right| \leq C \sum_{k > N} r_N^k$ . We shall reveal a contradiction from the integral  $\int |\partial_r q_T(r; a)| dr$  in Eq.(A.9).

For this purpose, it is first seen that  $r_T^{-[\alpha T]} (1-r_T) \rightarrow 0$  ( $T \rightarrow \infty$ ) for any  $0 < \alpha < 1$ . The same argument as in Eq.(A.9), with  $q_N$  replaced by  $q_{[\alpha T]}$ , gives

$$\int_{r_T}^1 |\partial_r q_{[\alpha T]}(r; a)| dr \leq C r_T^{-[\alpha T]} (1-r_T)^{\frac{\alpha+1}{2}} \leq C \left( r_T^{-\frac{2\alpha}{\alpha+1} T} (1-r_T) \right)^{\frac{\alpha+1}{2}} \rightarrow 0$$

as  $T \rightarrow \infty$ .

Before we proceed, a technical result is needed:

$$\left| \int f' \sin ktdt \right| \leq \frac{C}{k},$$

which can be verified by the equality

$$\begin{aligned} \int_0^{2\pi} f' \sin ktdt &= \sum_{j=0}^{k-1} \left( \int_{\frac{2j\pi}{k}}^{\frac{(2j+1)\pi}{k}} + \int_{\frac{(2j+1)\pi}{k}}^{\frac{(2j+2)\pi}{k}} \right) f' \sin ktdt \\ &= \int_0^{\frac{\pi}{k}} \sum_{j=0}^{k-1} \left[ f' \left( t + \frac{2j\pi}{k} \right) - f' \left( t + \frac{(2j+1)\pi}{k} \right) \right] \sin ktdt \end{aligned}$$

and the assumption that  $f'$  is of bounded variation.



Then an estimate of  $\int |\partial_r (q_T - q_{[\alpha T]})| dr$  yields

$$\begin{aligned} \int_{r_T}^1 |\partial_r (q_T - q_{[\alpha T]})| dr &\leq C \int \left| f'(t + \theta) \sum_{[\alpha T] < k \leq T} r^{-k} \sin kt \right| dt \\ &\leq C \sum_{[\alpha T] < k \leq T} r^{-k} \left| \int f'(t + \theta) \sin ktdt \right| \leq C \sum_{[\alpha T] < k \leq T} \frac{r^{-k}}{k} \\ &\leq Cr_T^{-T} \cdot \frac{1}{\alpha T} \cdot (1 - \alpha)T = Cr_T^{-T} \frac{1 - \alpha}{\alpha} \rightarrow 0 \end{aligned}$$

as  $\alpha \rightarrow 1$ . Therefore, we conclude that  $\int_{r_T}^1 |\partial_r q_T(r; a)| dr$  can be arbitrarily small as  $T \rightarrow \infty$  and  $\alpha \rightarrow 1$ , which contradicts the lower bound  $c > 0$  (see Eq.(A.8)). This completes the proof.  $\square$

## REFERENCES

1. Graham W. Alldredge, Ruo Li, and Weiming Li, *Approximating the m-2 method by the extended quadrature method of moments for radiative transfer in slab geometry*, Kinet. Relat. Models **9** (2016), no. 2, 237–249.
2. Eric Bertin, Michel Droz, and Guillaume Grégoire, *Boltzmann and hydrodynamic description for self-propelled particles*, Physical Review E **74** (2006), no. 2, 022101.
3. Thomas A Brunner, *Forms of approximate radiation transport*, Tech. report, Sandia National Lab.(SNL-NM), Albuquerque, NM (United States); Sandia . . . , 2002.
4. C. Chalons, R. O. Fox, and M. Massot, *A multi-Gaussian quadrature method of moments for gas-particle flows in a LES framework*, Proceedings of the Summer Program 2010, Center for Turbulence Research, Stanford University, Stanford, CA, 2010, pp. 347–358.
5. C. Chalons, R.O. Fox, F. Laurent, M. Massot, and A. Vié, *Multivariate Gaussian extended quadrature method of moments for turbulent disperse multiphase flow*, Multiscale Model. Simul. **15** (2017), no. 4, 1553–1583.
6. Christophe Chalons, Damieh Kah, and Marc Massot, *Beyond pressureless gas dynamics: Quadrature-based velocity moment models*, Commun. Math. Sci. **10** (2012), no. 4, 1241–1272.
7. Subrahmanyan Chandrasekhar, *Radiative transfer*, Courier Corporation, 2013.
8. Hugues Chaté, *Dry aligning dilute active matter*, Annual Review of Condensed Matter Physics **11** (2020), 189–212.
9. Pierre Degond and Sébastien Motsch, *Continuum limit of self-driven particles with orientation interaction*, Mathematical Models and Methods in Applied Sciences **18** (2008), no. supp01, 1193–1215.
10. Suresh M Deshpande, *A second-order accurate kinetic-theory-based method for inviscid compressible flows*, Tech. report, 1986.
11. J. R. Dorfman, Henk van Beijeren, and T. R. Kirkpatrick, *Contemporary kinetic theory of matter*, Cambridge University Press, 2021.
12. Lawrence C Evans, *Partial differential equations*, 2nd ed., vol. 19, American Mathematical Society, 2010.
13. Irene M. Gamba, Jeffrey R. Haack, and Sebastien Motsch, *Spectral method for a kinetic swarming model*, Journal of Computational Physics **297** (2015), 32–46.
14. Qian Huang, Yihong Chen, and Wen-An Yong, *Discrete-velocity-direction models of bgk-type with minimum entropy: I. basic idea*, Journal of Scientific Computing **95** (2023), no. 3, 80.
15. Qian Huang, Shuiqing Li, and Wen-An Yong, *Stability analysis of Quadrature-Based Moment Methods for kinetic equations*, SIAM J. Appl. Math. **80** (2020), no. 1, 206–231.
16. Qian Huang, Peng Ma, Linchao Cai, and Shuiqing Li, *Kinetic simulation of fine particulate matter evolution and deposition in a 25 kw pulverized coal combustor*, Energy & Fuels **34** (2020), no. 12, 15389–15398.
17. Thomas Ihle, *Kinetic theory of flocking: Derivation of hydrodynamic equations*, Physical Review E **83** (2011), no. 3, 030901.
18. M Cristina Marchetti, Jean-François Joanny, Sriram Ramaswamy, Tanniemola B Liverpool, Jacques Prost, Madan Rao, and R Aditi Simha, *Hydrodynamics of soft active matter*, Reviews of modern physics **85** (2013), no. 3, 1143.
19. Daniele L. Marchisio and Rodney O. Fox, *Computational models for polydisperse particulate and multiphase systems*, Cambridge University Press, Cambridge, 2013.
20. MATLAB, *version 9.5.0 (r2018b)*, The MathWorks Inc., Natick, Massachusetts, 2018.
21. Dimitri Mihalas and Barbara Weibel-Mihalas, *Foundations of radiation hydrodynamics*, Courier Corporation, 1999.
22. Gerald N Minerbo, *Maximum entropy eddington factors*, Journal of Quantitative Spectroscopy and Radiative Transfer **20** (1978), no. 6, 541–545.
23. M. Pigou, J. Morchain, P. Fede, M. Penet, and G. Laronze, *New developments of the extended quadrature method of moments to solve population balance equations*, J. Comput. Phys. **365** (2018), 243–268.
24. Gerald C Pomraning, *The equations of radiation hydrodynamics*, Courier Corporation, 2005.
25. L. Preziosi and L. Rondoni, *Discretization of the boltzmann equation and the semicontinuous model*, pp. 59–95.
26. Konrad Schmüdgen, *The moment problem. graduate texts in mathematics, vol 277*, Springer, Cham, 2017.

27. A Sengupta and C K Venkatesan, *On a discretised spectral approximation in neutron transport theory*, Journal of Physics A: Mathematical and General **21** (1988), no. 6, 1341.
28. Tamás Vicsek, András Czirók, Eshel Ben-Jacob, Inon Cohen, and Ofer Shochet, *Novel type of phase transition in a system of self-driven particles*, Phys. Rev. Lett. **75** (1995), 1226–1229.
29. V Vikas, Cory D Hauck, Zhi Jian Wang, and Rodney O Fox, *Radiation transport modeling using extended quadrature method of moments*, Journal of Computational Physics **246** (2013), 221–241.
30. Ke Yang, *Using the poisson kernel in model building and selection*, The Pennsylvania State University, 2004.
31. C. Yuan and R.O. Fox, *Conditional quadrature method of moments for kinetic equations*, J. Comput. Phys. **230** (2011), no. 22, 8216–8246.
32. Ruixi Zhang, Qian Huang, and Wen-An Yong, *Stability analysis of an extended quadrature method of moments for kinetic equations*, arXiv preprint arXiv:2306.07945 (2023).

DEPARTMENT OF MATHEMATICAL SCIENCES, TSINGHUA UNIVERSITY, BEIJING 100084, CHINA

Email address: chenyyho@mails.tsinghua.edu.cn

DEPARTMENT OF ENERGY AND POWER ENGINEERING, TSINGHUA UNIVERSITY, BEIJING 100084, CHINA

Email address: huangqian@tsinghua.edu.cn; hqqh91@qq.com

DEPARTMENT OF MATHEMATICAL SCIENCES, TSINGHUA UNIVERSITY, BEIJING 100084, CHINA, YANQI LAKE BEIJING  
INSTITUTE OF MATHEMATICAL SCIENCES AND APPLICATIONS, BEIJING 101408, CHINA

Email address: wayong@tsinghua.edu.cn

DEPARTMENT OF ENERGY AND POWER ENGINEERING, TSINGHUA UNIVERSITY, BEIJING 100084, CHINA

Email address: 1553548358@qq.com